CODEN:LUTEDX/(TEIE-5474)/1-84(2022)

Industrial Electrical Engineering and Automation

Solar Energy Harvesting for Outdoor Applications

A Technical Feasibility Analysis

Jonatan Andersson
Kristoffer Kjaerran

Division of Industrial Electrical Engineering and Automation
Faculty of Engineering, Lund University

LUNDS
UNIVERSITET

Solar Energy Harvesting for Outdoor Applications

A Technical Feasibility Analysis

Jonatan Andersson

Kristoffer Kjaerran

Supervisor: Gunnar Lindstedt
Examiner: Ulf Jeppsson

Industrial Electrical Engineering and Automation, LTH

Abstract

The use of solar cells as a solution for different energy harvesting applications has seen a significant growth during the last few years. With recent advances in the power conversion efficiency and manufacturability of organic photovoltaic cells these systems can be made even cheaper and more available for consumers, opening up new ways for solar technology to be implemented into products.

This project investigates how an energy harvesting system suitable for low power applications can be constructed with the use of an organic photovolatic cell as the energy harvesting source. It also explains how this energy is sampled via a regulatory integrated circuit chip and how this all is connected via a PCB. All components were carefully evaluated, tested and assembled to form a final energy harvesting system.

The project also resulted in a simulation tool that can simulate the performance of the energy harvesting system as implemented in a specific battery charging application. From these simulations it is concluded that the system is very dependent on the organic photovoltaic cell azimuth angle. It performs well in south facing harvesting, allowing for a substantial battery charging potential, but struggles to provide charging power for a north facing OPV. However, depending on the magnitude of draining current of the battery, a north facing OPV can still provide enough charging current to be considered feasible for implementation. The report concludes that from a performance point of view, an OPV based energy harvesting system can extract enough energy to provide real value for potential future Verisure products.

Acknowledgements

To start of we would like to thank Verisure for giving us the opportunity to write a master thesis with them. A special thanks goes out to our supervisor Nick Hackett for guiding us troughout the project and always doing his best to help us with resources and other requests. We are also grateful for the large amount of help and knowledge from Igor Jankiewicz and Balamurali Radhakrishnan regarding the PCB design and any electronics related questions.

At Lund University we would like to thank Henrik Davidsson for his sharing expertise on solar power, helping us solve problems and giving us access to the university solar lab facilities. Lastly a big thanks to our supervisor Gunnar Lindstedt for keeping us in line with all the requirements from Lund University.

Acronyms

BOM Bill of material.

C Capacitor.

CRON Time-based job schedule.

D Diode.

EHS Energy harvesting system.

ELCD Electrical double layer capacitors.

FOCV fractional open circuit voltage method.

HH Hours solar time.

HOMO Highest occupied molecular orbit.

IC Integrated circut.

ICA Incremental conductance algorithm.

IV-Curve Current-Voltage curve.

L Inductor.

LOMO Lowest occupied molecular orbit.

MM Minutes solar time.

MPP Maximum power point.

MPPT Maximum power point tracker.

OCV Open circuit voltage.

OPV Organic photo voltaic.

PC Polycarbonate.

PCB Printed circut board.

PCE Power conversion efficiency.

PnO Pertube and Observe.

PV Photo voltaic cell.

S Switching.

SI derived International system of units derived.

STC Standard test conditions.

Contents

1 Introduction

1.1 Background

Verisure is a company that delivers complete home security systems. In order to simplify the installation process of these systems and to be able to provide as many people as possible with home security, most of Verisures detection devices, are powered with batteries, meaning that no new power has to be drawn for node installation, allowing the customer a greater freedom of placement. In a strive to become more environmentally friendly and to provide customers with even more freedom of placement of the detector nodes, Verisure wants to explore what solar cell technology can do in terms of harvesting usable solar energy. Using organic photo voltaic (OPV) cells to harvest energy, the goal of this project is to study the possibilities for how solar energy harvesting can be implemented, how the energy can be stored and how later used.

1.2 Project Description

As new photo voltaic (PV) technologies emerge, new possibilities and areas of use emerge with them. OPV cells is one of these new technologies and have a few attributes that make them very interesting for use. Two of the properties that makes OPVs desirable to study in depth, are their mechanical flexibility allowing for innovative ways of mounting them. Their relatively low production cost, also makes them worth while integrating in more low cost applications.

This project is an in depth study of how a specific OPV provided by Verisure performs in an outdoor setting and how it can be implemented in a device as a complete energy harvesting system (EHS). The project will have an evaluating part, where the OPV's performance is charted and its properties understood in order to make further decisions regarding the EHS. The evaluation part will also consist of the evaluation of potential components that may be included in the EHS in order to find the optimal configuration for the final implementation. When the EHS is defined, the exact performance can be studied, allowing for a better understanding of the energy losses in the system. Lastly, the EHS can be simulated for different user scenarios. Depending on the way the EHS is configured and how the harvested energy is used, different simulations can be set up. Since the energy output of the OPV will be different depending on where it is used geographically, different coordinates can be simulated to study the difference in performance.

1.3 Objectives

- Get an understanding for the exact performance of the considered OPV in conjunction with our design of PCB while operating in a device with no compromises in its proposed physical design.
- Identify the limitations of the OPV while operating in non ideal conditions.
- Design an electric circuit to rectify the OPV output in order to charge the energy storage unit and implement this into a printed circuit board (PCB) design.
- Manufacture an actual prototype of the PCB design to the specific form factor suggested by Verisure.

1.3.1 Design Limitations

In order to conduct this project, a set of design parameters must be defined to properly scale and design the Energy Harvesting System. This ensures that the outcome of the project is relevant to all parties included. The restrictions are as follows.

- The active area of the OPV can not be larger than 55mm x 53mm.
- The assembled PCB must be contained within a volume of 10mm x 30mm x 2.5mm.
- The OPV should be non-flat.
- The OPV should be installed in a non-tracking way. Meaning that the OPV should not track the optimal azimuth angle.
- The zenith angle of the OPV should be 90°.

As stated above, the studies conducted on the OPV should be non flat. The motivation for this is to utilize the flexible properties of the OPV to explore the performance of in a non-flat scenario and to provide more flexibility in installation.

1.4 Division of Labour

A presentation of work done on different parts of the project can be seen below.

Kristoffer Kjaerran
Report: Introduction **(1.1, 1.2, 1.3)**, Theory **(2.3)**, Component Evaluation **(3.1, 3.2, 3.3, 3.6, 3.7)**, PCB Design **(4.1, 4.2, 4.3)**, Power Output and Battery Charging Simulations **(5.1, 5.2.2, 5.2.3)**. **Other tasks**: PCB design, Soldering Components, Indoor and Outdoor OPV Experiments, Solar Simulations.

Jonatan Andersson
Report: Theory **(2.1, 2.2)**, Component Evaluation **(3.4, 3.5)**, Power Output and Battery Charging Simulations **(5.2,1 5.2.2, 5.2.5)**. **Other tasks**: Indoor and Outdoor OPV Experiments, Solar Simulations, Soldering Components.

Other parts of the report were a common effort.

2 Theory

In this section, a brief introduction of the technologies present in this project is presented. The necessary areas, such as different solar cell technologies, solar data and how it is interpreted, along with how energy harvesting systems usually is configured is some of the subjects treated.

2.1 Solar Panels

2.1.1 Introduction

In 1839 the first evidence of a PV effect was discovered by a 19-year old physicist by the name Alexandre Becquerel. When working with electrodes in his fathers laboratory he discovered that the current between them increased if the materials were illuminated. Becquerel was using a Platinum electrode coated with silver chloride and silver bromide for his experiment. The working principle behind this was unknown until Albert Einstein described the phenomenon in 1905, which later won him the Nobel price. Solar cells continued to develop throughout the years and the silicone based PV cells soon came to be the dominant force on the market, being well regarded for its high efficiency and long lifespan. During this time, efficiency has also skyrocketed from 2 percent in 1955 to 47.1 percent in 2019. In the late 80s, a solar cell using organic compounds was launched by Michael Grätzel and Brian O'Reagan known today as OPV (Organic Photovoltaic cell). It offered significant reduction in manufacturing cost but came with a large trade off in efficiency. [34]

As stated, photovoltaic cells (PV) also known as solar cells have seen an explosive expansion in the last decades where green energy and climate change have become central questions for many countries. This has lead to many new varieties and applications for the PV cell. Some big challenges with PV cells though is their uncertainty and unreliability to produce a dependable power output. This makes it redundant to use only PV cells as a power source for certain purposes. A new use has therefor emerged where PV cells are used as a "support" power supply. This means that a device might run on batteries and use solar power to recharge its batteries. Physical location also plays a big part in the usefullness of solar cells as the amount of sun hours per year often dwindles the further away from the equator the location is. Another important factor is the way the solar cells are installed. Angle towards the sun, also known as the zenith angle (an angle between the plane and its normal), and the Azimuth angle, the angle between the current position and north, is vital parameters for optimal power output. These can be seen in figure 1 [22].

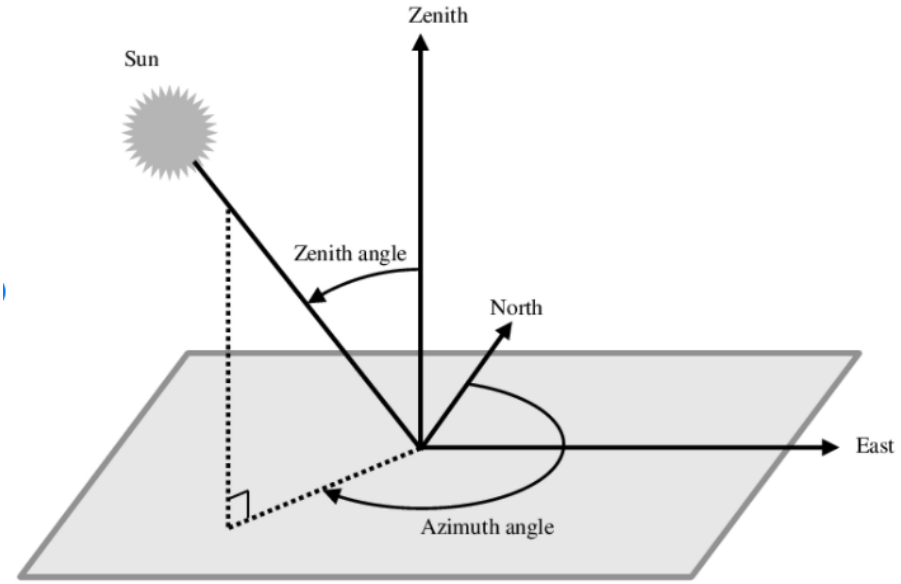

.

Figure 1: Zenith and Azimuth angles [29]

.

2.1.2 Spectral Range of Light Sources

Sunlight is made up of many different wavelengths of light where the viable range is 400 to 700nm. PV cells typically make use of this whole spectrum and often beyond these wavelengths, such as infrared light. Solar cell performance can also vary depending on the spectral range. Some are more efficient at low wavelength, some at higher, depending on the PVs unique absorption range. This means that to simulate their behaviour in sunlight a lamp with a similar wavelength distribution as daylight is needed. As seen in figure 2 and 3, do some light sources do not represent daylight very well, for example a halogen lamp does not replicate sunlight well. Instead a lamp specially designed for the purpose of testing outdoor solar cells should be used. A sulfur plasma lamp is commonly used for this appliance since it replicates the visible wavelengths of solar radiation quite well. Its spectral analysis can be seen in figure 4. One down-side of these lamps is their slightly lower infrared irradiance and higher for the 450-550nm wavelength. With that said, sulfur plasma lamps are often seen as good enough and do not have the electron spikes in their wavelength spectrum like led lamps have, or the shift of its wavelength spectrum towards the IR range like halogen light sources[3].

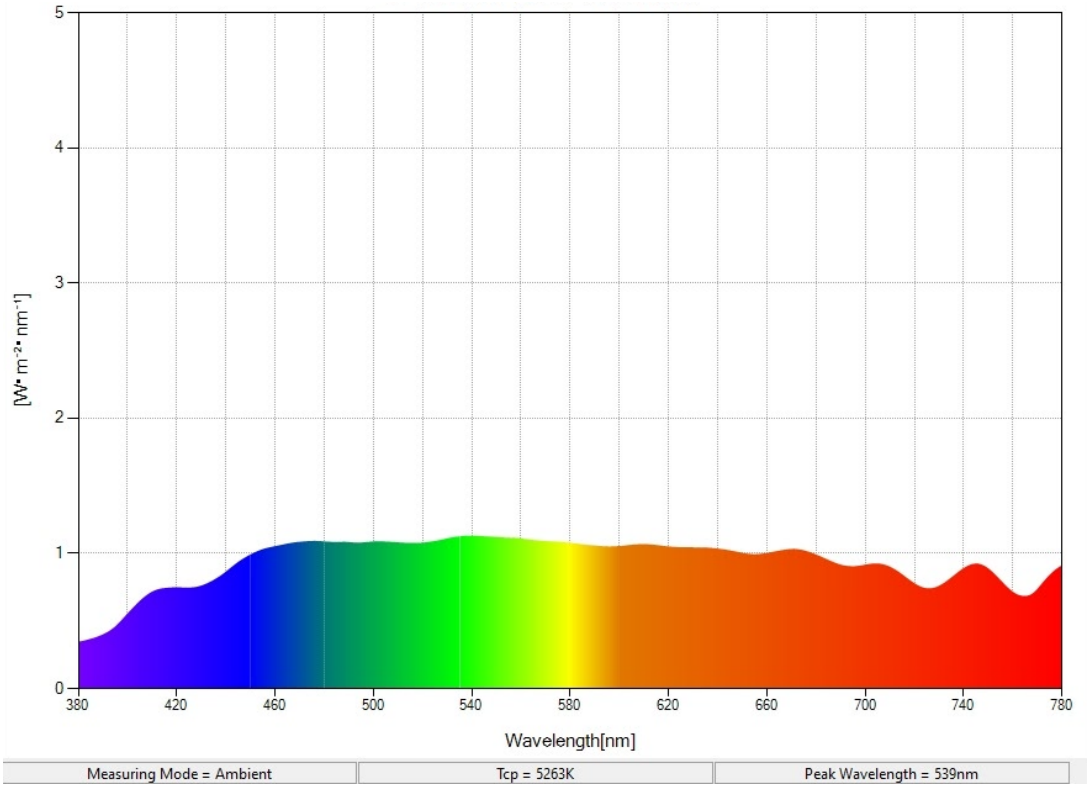

Figure 2: Spectral analysis of sunlight

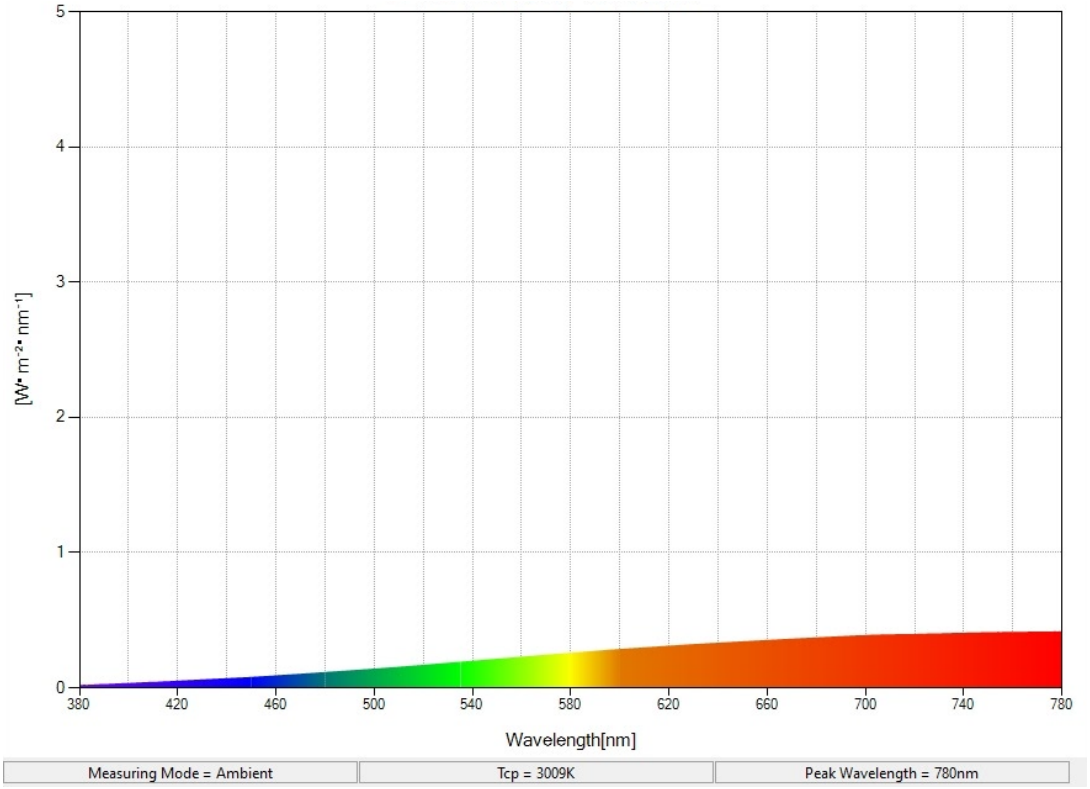

Figure 3: Spectral analysis of a halogen lamp

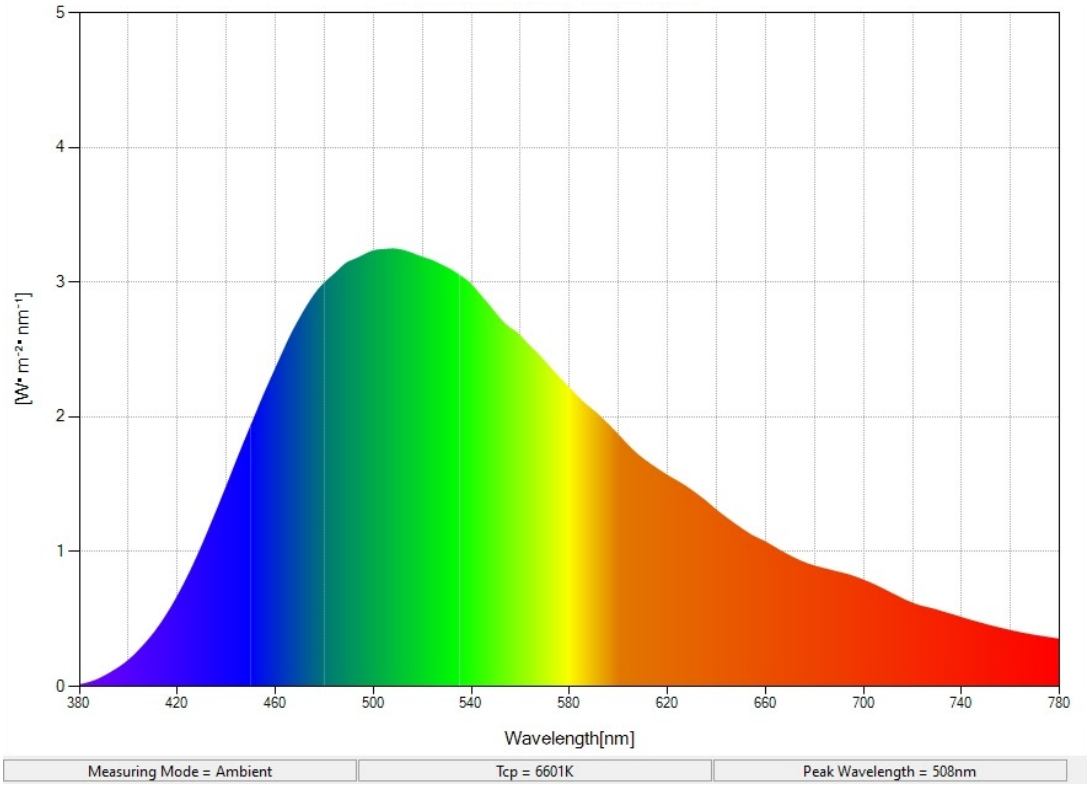

Figure 4: Spectral analysis of a plasma lamp

2.1.3 Working Principle

The most common way to construct a PV cell is with a so called PN-junction. This is often done using high grade silicone with a purity over 99 percent as a semiconductor. The silica forms into crystals where each of the 4 valence electrons bonds with other silica atoms in their surroundings. When the crystalline structure has been formed the Silica will be "doped" in different layers. Doping in itself is a complex process but explained in simple terms it is an addition of impurities to an existing semiconductor. In the PN-Junction the doping using phosphorous results in a n-type semiconductor and doping using bromine generates a p-type semiconductor. Phosphorus has five valence electrons and when doping silica with it a medium for electrons to move will arise. This is possible since only four of the five valance electrons can bind with the silica's four. As for bromide the same principle is in work but inverted. Bromides 3 free electrons can not bind with the 4 of silica's. The result is a so called "hole" where no electron is bonded and can be viewed as a positive charge. The area where these two types of semiconductors meet is called a "depletion zone" seen in figure 5. Electrons from the n-type will soon start to diffuse into the p-type in order to fill these positively charged "holes". When electrons migrates from the n-type to the p-type they leave behind + charges holes and also gives a - charge to the p-type. This will cause the depletion zone to have a current since the n-type is positively charged and the p-type negatively charged. This current will induce an electrical field [1] [11].

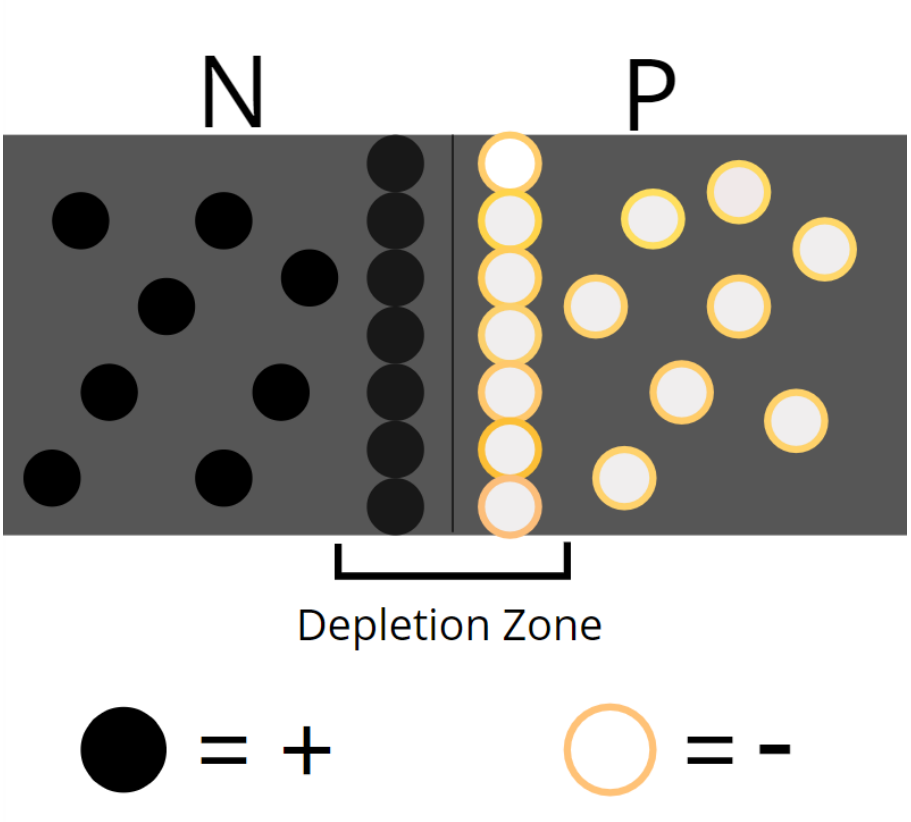

Figure 5: A p-type and a n-type semiconductor generating a depletion zone

Illuminating the depletion zone will cause hole and electron pairs to arise, these pairs would rapidly bind together again under normal circumstances but the electrical field will cause the electrons to go towards the n-type transistor and holes towards p-type given their charge. If a connection is made from the n-type and p-type material the electrons will flow from the n-type to the + charged holes in the p-type resulting in a current [1] [11].

2.1.4 Organic Photovoltaic Cells

An OPV uses the same basic principal as traditional PV cells, separating electrons and holes to generate a voltage. Although the methods are similar the structure of these cells varies greatly. A PN-Junction is also used in OPVs consisting of a donor (P-material) and acceptor (N-material) respectively where the donor-acceptor interface separates "excitons". Excitons consist of an electron in the lowest occupied molecular orbit (LUMO) and a hole in the highest unoccupied molecular orbit (HOMO) and exist for a few nanoseconds when the donor material is excited by light. When diffusing through the donor-acceptor layer the electron is separated through the acceptor and the hole remains in the donor. Similar to what is described in section 2.1.3. Organic materials is used for the donor and acceptor from where OPV derives its name. A lot of different carbon based materials are used for OPV but the common factor is that polymers or fullerens often make up the donor and acceptor part. For optimum efficiency the surface area in-between the acceptor and donor should be maximised. Taking cost into consideration a trade off often have to be made. Today there are three main versions used seen in 6 and 7 [22].

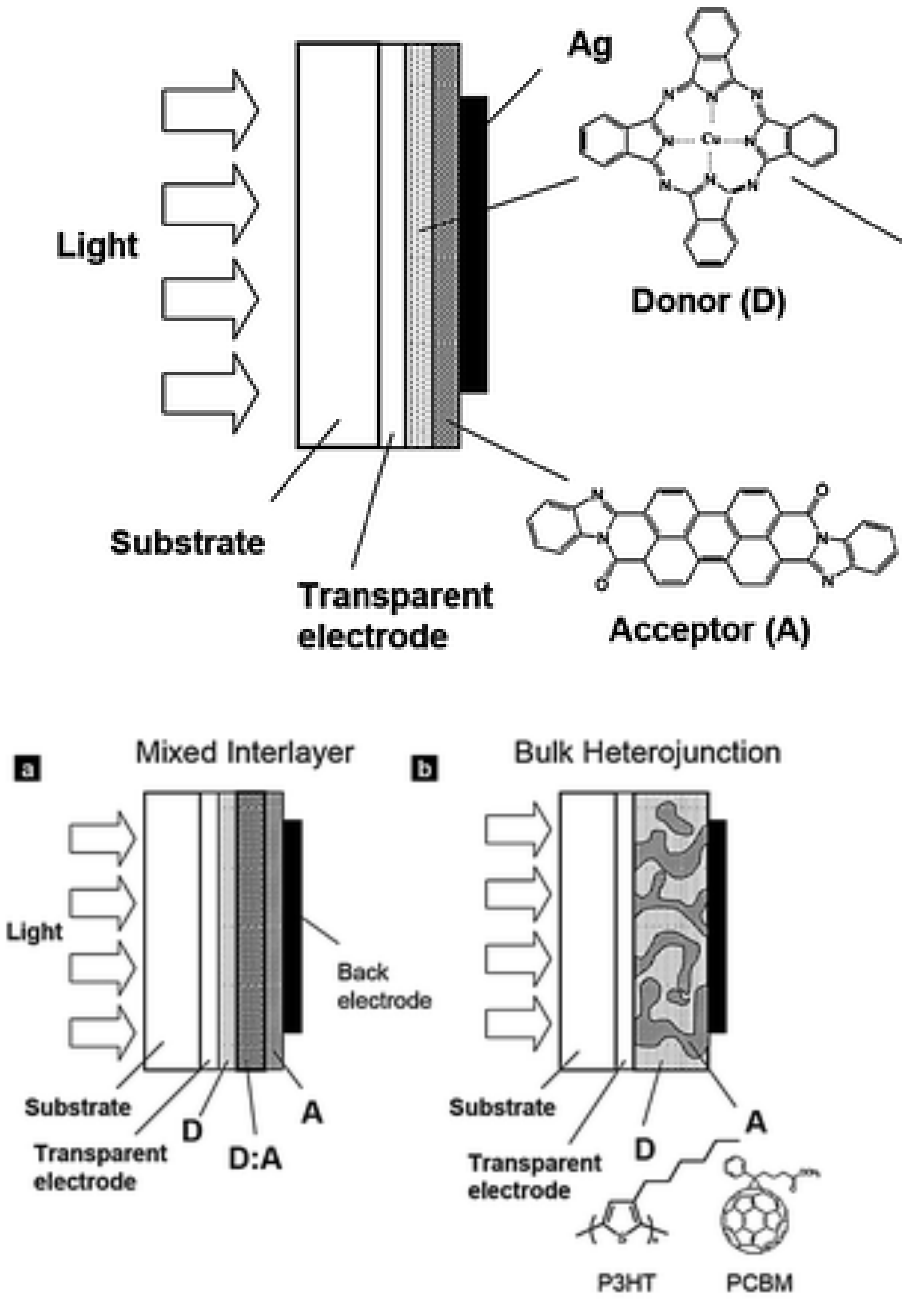

Figure 7: OPV with mixed interlayer and hetrojunction [12]

Manufacturing cost for OPVs can be pushed down significantly from ordinary silicon based PV Cells. This is much thanks to the roll-to-roll printing used and the low cost of material. The roll-to-roll printing techniques are many, and still evolving into a processes that can support mass production. Many of the techniques are in use in other industries and some can for example be found in newspaper manufacturing where ink, the motif, is transferred to paper, the substrate. The roll-to-roll processes can look similar, where the polymer or fullerens are makes up the active layer, acts as the motif and the substrate is whatever exterior encapsulating the polymer active layer. Prior to roll-to-roll printing, spin coating was often used, which can not be industrialized to the same degree. Toxic and environmentally hazardous

chemicals can also be eliminated from the manufacturing process [26]. Some other properties of OPV are their high mechanical flexibility and option to use different colours in their dye when being printed. There is also some major drawbacks to OPVs with the biggest one being the low efficiency. With a max efficiency record of 18.2 % compared to the Silica based PV cell record of 47.1 %. Ordinary OPVs on the market have a hard time keeping up with the state of the art OPVs though and therefore often have a lower efficiency somewhere in between 2-10 percent [22] [19].

2.1.5 OPV Stability in Outdoor Environments

One of the major inhibiting factors of implementing and using OPV technologies, is their relatively bad chemical stability during long time use. This means that compared to other PV technologies, such as the conventional, silicon based PVs, the OPV cells are more susceptible to degradation due to external factors, such as exposure to water, oxygen and radiation. Since OPV research is young, studies regarding the actual lifetime of the OPV cells are still lacking. However, the extrapolated results from the studies that have been made, show a potential lifetime of 10-15 years for some OPV technologies. The degradation experienced throughout the life of an OPV cell is often divided into the initial "burn in" period, where an exponential degradation of the power conversion efficiency (PCE) in the OPV can be seen, and the rest of the lifetime of the OPV cell, when a slower but linear decrease can be seen. The burn in period often lasts around 100 hours [18] or under, during irradiance exposure while the lifetime itself is defined by the point where the PCE of the OPV is 80% of what it was at the end of the "burn in" period [27].

Many different processes are contributing to the degradation of OPV cells, both chemical and mechanical. One of the most important things to do, to protect the OPV cells from degradation, is proper encapsulation of the cells. This could for example be a glass-on-glass encapsulation, where the OPV cells are fixed between two glass layers, or a flexible film barrier encapsulation, where the cells are placed between two layers of a transparent, flexible film. This protects the cell from the exposure to oxygen and moisture. Proper encapsulation of the cell is what allows lifetimes of 10 years and greater. Even if proper encapsulation is key for long lifetime, it does not help with preventing burn in, since that is a result of illuminating the photo active area of the cell. The burn in phenomenon instead needs to be prevented by other means, such as advances in manufacturing. The burn in period has a potential to reduce the initial PCE of the cell by 10-50% and is one of the major problem in sustaining the PCE [18].

2.1.6 Absorption Spectrum of OPV

An absorption spectrum of an OPV is shown in figure 8. From this figure it can bee seen that its PCE is dependant on the wavelength of the incident light.

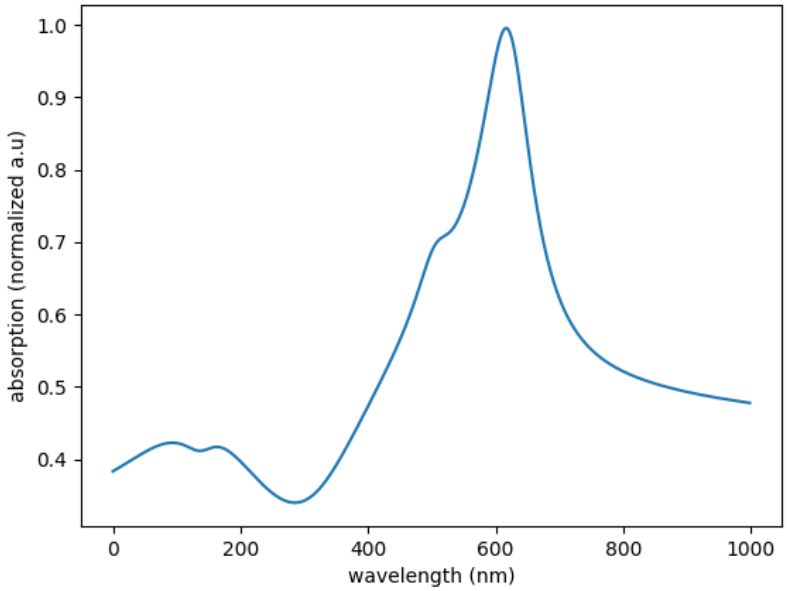

Figure 8: Absorption range of an OPV module.

2.1.7 Solar Cell Equivalent Circuit

PV cells can be represented in the form of an electric circuit where the cell is modeled as a current source, representing the solar cell being hit by light and PN-diode representing the working principles of the PV cell. In reality, parasitic resistances will always be present in the circuit. In the most simple electrical representations of a PV cell, only a parallel resistance, called a shunt resistance(R_{sh}), and a series resistance(R_s), are added relative to the current source. An illustration of this equivalent circuit is shown in figure 9.

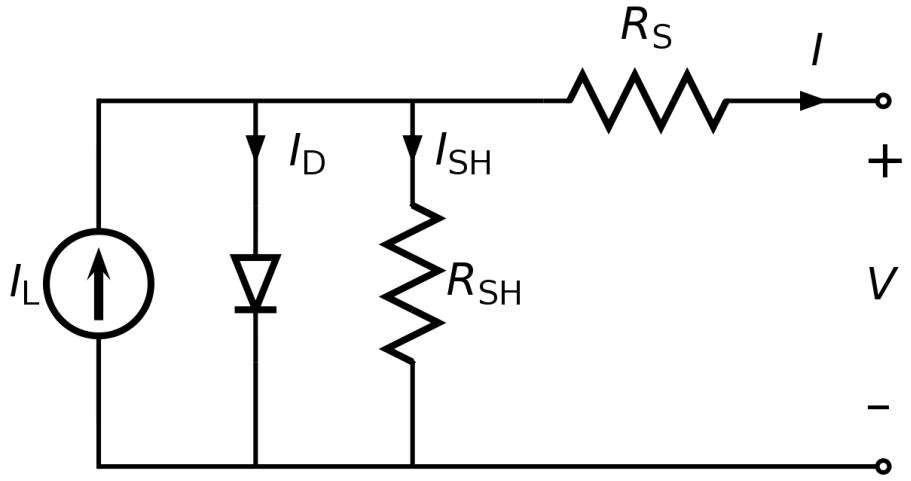

Figure 9: Circuit representing the electrical properties of a PV cell

The two parasitic resistances will ultimately limit the cells performance. An ideal PV cell would be equivalent to solely a current source in parallel with the diode. The ideal case in other words be represented as the equivalent circuit shown in figure 9 but with an infinitely large shunt resistance and

a series resistance equal to zero. However, as the shunt resistance decreases or the series resistance increases, the performance of the PV cell decreases.

The shunt resistance originates from microscopic defects, called shunt defects, in the PV cell that allow for an alternative path for the generated photocurrent to flow through. These defects contribute to lowering the shunt resistance. In the IV curve, lowering of the shunt resistance results in a more negative slope at the short circuit current density point (Isc). This will decrease the fill factor of the maximum power point. The fill factor is a measurement defined as $FF = (V_{mpp} * I_{mpp})/(V_{oc} * I_{oc})$ and is a measurement describing the "squareness" of the IV curve. A higher FF usually means the performance, in the form of PCE, of the OPV is better. Refer to fig. 17 for a visual representation of the notations above. The series resistance originates from the metal output contact points having an internal resistance, or from the leads connected to these contacts. An increase of these resistances decreases the negative slope in the IV curve at the open circuit voltage point (Voc). This will also decrease the fill factor of the MPP [25] .

2.1.8 Photoactivation of Organic Photovoltaic Cells

When stored in dark compartments or in contact with oxygen, additional shunt resistance is introduced to a OPV. The effect of these problems is described in section 2.1.7. When exposed to light, OPV cells undergo a process called photoactivation, in which the structure of the active layer in the OPV changes its structure, which eliminates the shunt resistance related to this phenomenon. The sub-optimal performance and behavior of the OPVs before photoactivation can be seen on a IV curve as a flattening of the curve, decreasing the otherwise characteristic "knee" or "hip" of the curve where it normally would change in tilt, as expected of a diode IV curve. To photoactivate an OPV fully it needs to be exposed to high intensity radiation for up to 24 hours depending on the cell used. If left in darkness for a long period of time this process can reverse again, introducing the shunt resistances and decreasing the fill factor [4].

2.1.9 Efficiency

The efficiency of a solar cell, often called the power conversion efficiency (PCE) is defined as seen below. This is an important metric as it determines the active area of a PV cell needed to output a certain power.

$$\eta = \frac{P_{max}}{P_{in}} \tag{1}$$

where P_{in} is equal to area A (m^2) multiplied by the indecent radiation flux E (W/m^2) and P_{max} is achived at the MPP (maximum power point).

$$P_{in} = A * E \tag{2}$$

$$P_{max} \; at \; the \; MPP \tag{3}$$

[19][33].

2.1.10 Standard Testing Conditions for Solar Cells

In order to compare the performance of different solar panels, a set of testing conditions have been determined as an industry standard. These standards are defined as follows:

- The temperature of the cell must be 25 °C
- The irradiance affecting the surface of the cell must be 1000 W/m^2
- The air-mass value must be 1.5, meaning that the test should simulate sun-rays traveling at an 45 deg angle through the atmosphere

It is important to note that these testing conditions do not represent a common real world scenario very well. For example, for these kind of irradiance levels, the surface on the solar cells tends to be much warmer. The standard is only set as a way to compare solar panels. It is also true, that the STC conditions are strict and many PV manufacturer's internal testing are still lacking in consistency as they use different lamps and measuring setups to test their panels. This downgrades the validity of the STC ratings of PV cells [33].

2.2 Solar Radiation

2.2.1 Different Solar Data

Light is often measured in illuminance or irradiance and there is a fundamental difference between these two measurement units. Illuminance is measured in the SI derived unit "Lux" and represents the total incident luminous flux on a area. Lux can be connected to another SI derived unit "lumen" where 1 lux equals 1 lumen per square meter. When measuring Lux a function weighted towards the human brightness perception is used. A side effect of this is that some wavelengths will contribute more to the illuminance reading than others. Therefor Lux is a unit of measurement often used for indoor readings to get the perceived brightness of lamps, tabletops, etc. But also for indoor solar panels. Irradiance on the other hand is a measurement of the power in light that hits a specific area (radiant flux) and has the unit W/m^2. Outdoor solar panel testing often use irradiance as it does not use the luminosity function used to measure illuminance. Since the unit is "power per square meter" irradiance often is used to easily calculate the PCE of a solar cell, meaning how much of the power in the light hitting the solar cell is converted into useable energy.

When extracting solar data it is often retrieved as its three different components, which together make up the total irradiance value at a certain time at a certain location. One of these components is the direct, or beam, irradiance G_b being the light that originates directly from the light source to the affected area. Second is the diffused irradiance G_d that can be described as the light scattered in the clouds and other particles in the atmosphere. The third one is reflective irradiance G_r. This is caused by light reflecting on different surfaces and will vary depending on the surrounding geometry and material that the light reflects on. Zenith angle will make a significant impact on reflective irradiance since an angle of 0 degrees will cause it to be 0 as no light hitting the ground can be deflected on a surface facing away from the ground [32].

$$G = G_b + G_d + G_g \tag{4}$$

This will be further explained in the coming sections.

2.2.2 Calculation of Solar Angels

In order to calculate the effective radiation for a specific surface, at a specific location at a given time without empirical testing, the angle of incidence of the direct beam to said surface must be derived. The goal of this derivation is to create an expression for the angle of incidence of the beam radiation, θ, that later can be used to calculate the effective radiation.
To start off a zenith vector is defined as running through the north pole, a south axis along the equator and a west axis going orthogonality to these two, see figure 10. After this a local coordinate system is also defined by rotating the global system and choosing a place of interest to study. By doing this all the local coordinates can be defined by the global system. Lastly a solar vector R can be defined.

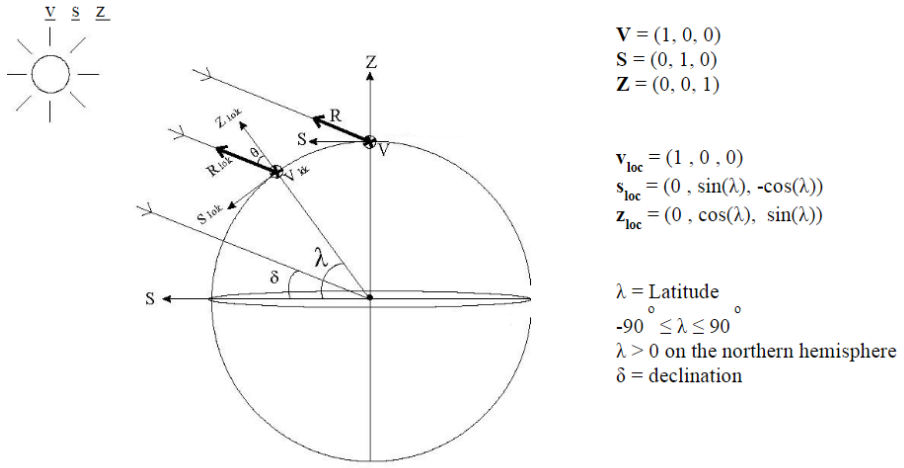

Figure 10: The global and local coordinate systems, latitude λ and declination δ is also shown

By then calculating the hour angle ω and using δ, R can be defined, see figure 11.

$$\mathbf{R} = (\cos(\delta)\sin(\omega), \cos(\delta)\cos(\omega), \sin(\delta))$$

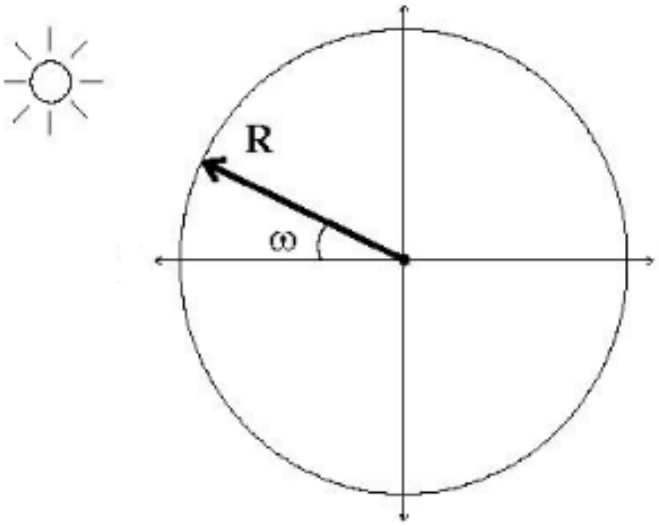

Figure 11: Hour angle and coordinates of R projected on the horizontal plane

The hour angle can also be described as the angular displacement of the sun, west or east from the local meridian caused by the earth's rotation. The rotational speed is 15° per hour and ω is set to 0 at 12:00 solar time and positive thereafter. This means that -180° < ω < 180°. To calculate ω a simple equation can be used were HH is the hour and MM is the minute for solar time.

$$\omega = ((HH - 12) + MM/60) * 15(degrees) \tag{5}$$

Declination, δ, is the angle between the sun and equator, since the earth's tilt is 23.45° δ can vary -23.45° < δ < 23.45° depending on the season. It is set to positive when then sun is north of the equator meaning after Spring equinox and before Autumn equinox. Just as the hour angle this can be simplified into an equitation

$$\begin{aligned} \delta &= 23.45 sin(360(284 + n)/365) \\ n &= \text{daynumber specific year} \end{aligned} \tag{6}$$

Projecting R can now also be done. Since δ is the angle between R and S-V plane the z component of R is sin(δ). Using the solar angle ω, s and w components can also be calculated resluting in the projection of R as seen in figure 11.

In order to calculate the components of the solar vector R in the local coordinate system the scalar product between R and the axis unit vectors, $V_{lok}, S_{lok}, Z_{lok}$, are used.

$$
\begin{aligned}
R_{lok} &= (R \cdot V_{lok}, R \cdot S_{lok}, R \cdot Z_{lok}) \\
&= (cos(\delta)sin(\omega), (cos(\delta)sin(\omega)sin(\lambda) - sin(\delta)cos(\lambda), \\
&\quad cos(\delta)cos(\omega)cos(\lambda + sin(\delta)sin(\lambda)
\end{aligned} \tag{7}
$$

The normal plane, N, in the local coordinate system can be described as:

$$
\begin{aligned}
N &= (sin(\beta)sin(\lambda), sin(\beta)cos(\gamma), cos(\beta)) \\
\beta &= \text{tilt of the surface from the horizontal}, 0 < \beta < 180 \\
\gamma &= \text{rotation from south(azimuth)}, -180 < \gamma < 180
\end{aligned} \tag{8}
$$

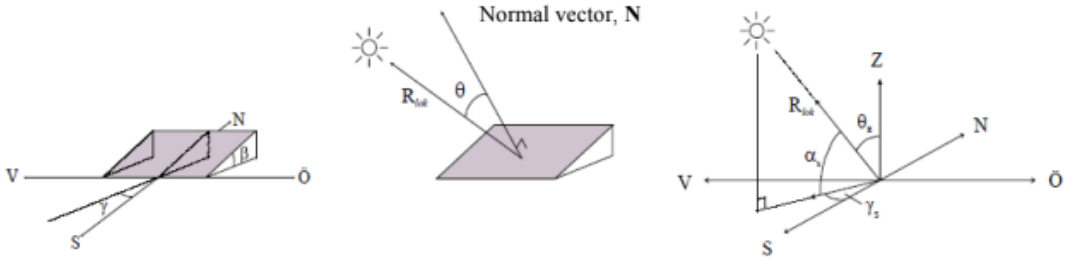

.

Figure 12: Left figure shows the tilt β and the azimuth angle γ. Middle figure shows the normal vector and the angle of incidence θ. The rightmost figure shows 3 new parameters that will be used in later calculations: solar azimuth γ_s, solar height α_s and zenith angle θ_z

Finaly, after defining all these parameters the incidence angle θ can be determined as:

$$
R_{lok} \cdot N = cos(\theta) \tag{9}
$$

$$
\theta = arcos(R_{lok} \cdot N) \tag{10}
$$

Solar azimuth, γ_s, and solar height, α_s, can also be used to calculate R_{lok} as:

$$
R_{lok} = (cos(\alpha_s)sin(\gamma_s), cos(\alpha_s)cos(\gamma_s), sin(\alpha_s)) \tag{11}
$$

where γ_s = south and the projection on the ground plane of the sun -180° < γ_s < 180° and
α_s = Solar height angle 0°<α_s < 90°[5].

2.2.3 Effective Irradiance

Solar radiation can be separated into 3 different forms. The most significant of these are direct and diffuse radiation. Shown in 13

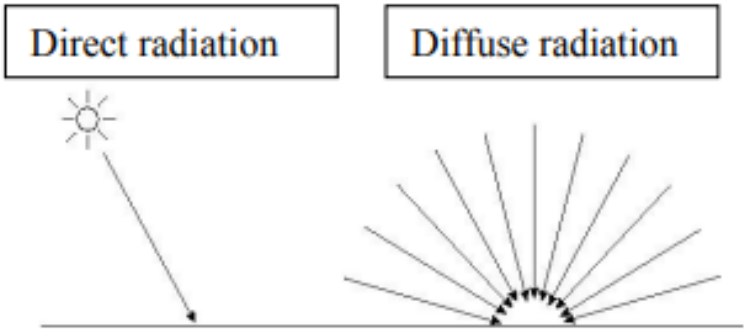

Figure 13: Direct and diffuse radiation. The atmosphere will diffuse the solar radiation and cause some photons to scatter resulting in diffuse radiation.

Some parameter will now be introduced in order to calculate different scenarios. Indices will also be used where *b*= beam, *n*= normal,*andh*= horizontal.

G_d= diffuse radiation, G_b = direct (beam) radiation:

$$G_b = G_{b,n} cos(\theta) \tag{12}$$

$$G_{d,h} = G_h - G_{b,h} \tag{13}$$

$$G_{b,h} = G_{b,n} cos(\theta_z) \tag{14}$$

$G_{b,n}$ = direct radiation towards the surface perpendicular to the surface
$G_{d,h}$ = diffuse radiation towards a horizontal surface
$G_{b,h}$ = direct radiation towards a horizontal surface
G_h = total radiation towards a horizontal surface
θ_z = Zenith angle

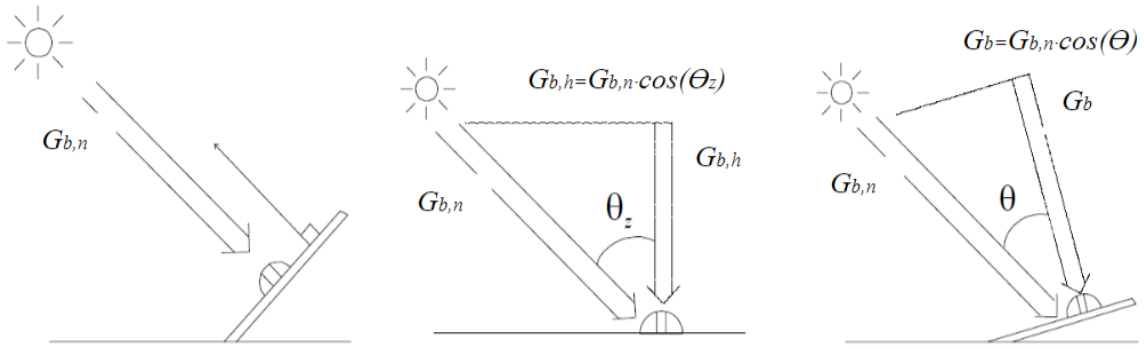

Figure 14: Visualisations of different radiations. Left shows $G_{b,n}$, middle shows $G_{b,h}$ and right shows the direct radiation G_b.

Lastly ground reflected radiation, G_g, should also be taken in to consideration.

$$G_g = \rho_g G_h (1 - cos(\beta))/2 \tag{15}$$

ρ_g = reflectance of the ground
$(1 - cos(\beta))/2$ = the surface of the plane as seen from the ground
Using all defined parameters the effective radiation can be calculated.

$$G = G_b + G_d + G_g \tag{16}$$

Their is often beam and diffuse radiation data available for any given place on earth via various institutions or websites [5].

2.3 The Energy Harvesting System

2.3.1 Introduction

A solar energy harvesting system can be implemented in a variety of different ways. In most cases however, the need to optimize the energy harvesting potential is crucial, resulting in efficiency demands of the EHS. Going through the chain of energy transfer in an EHS starts with the working principle of the PV where energy from light radiation is harvested. The output from the solar panel is dependent on irradiance levels and cell temperature, making the PV output uneven. A DC-DC converter is therefore used in order to regulate the magnitude of the voltage supplied as many energy storage units requires an even or constant voltage for charging purposes. The DC-DC converter will also have to receive input from a regulating circuit called a "maximum power point tracker" (MPPT) that informs the DC-DC converter on how to adjust the voltage output to maximize the power output. The output from the DC-DC converter is then supplied to the energy storage unit. Depending on what energy storage unit is used, a discharge and overcharge circuit might be needed to protect the unit. The choice for energy storage unit will also dictate whether a second DC-DC converter must be used for a mismatch in voltage output from the energy storage unit and desired voltage input to the load that is to be powered, to be avoided [23]. A diagram showing the components included in the energy harvesting circuit is seen in figure 15.

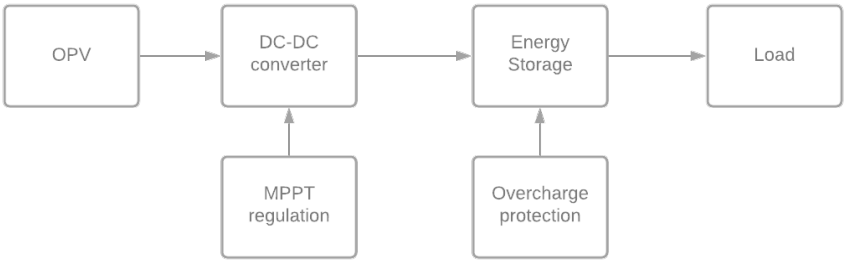

Figure 15: System overview of the energy harvesting components

2.3.2 DC-DC Converters

For managing the uneven voltage output from the solar panels, a DC-DC converter is often used to alter the magnitude of said voltage. In an energy harvesting application, where the voltage output from the energy source is generally low, a boost converter can be used to convert the OPV output voltage to the

voltage needed for the application. The application can vary and a DC-DC converter can be used for several different operations. For example, the application can be the charging an energy storage unit.

The working principles of a boost converter in its most simple format is achieved with only three electrical components. These are one inductor (L), one capacitor (C) and a switching (S) component, such as a MOSFET or other transistors. The circuit uses the fact that an inductor tends to want to withstand changing in current flowing through it, by instead change the magnetic field around it. When the converter is in its on state, with the switching device closed, the polarity of the voltage input wants to increase the current through the inductor and the inductor responds by increasing its magnetic field. When the converter is in its off state, and the switching device is open, the polarity of the inductor switches and the stored up energy in the inductance decreases. At this moment, the voltage source and the inductor are in series, making the combined voltage drop over the inductor and voltage source greater than the voltage source. this is what allows a boost converter to output a higher voltage than what is put in. In figure 16 a simple circuit diagram of a boost converter is seen. The diagram includes a fly-back diode (D) that is present to inhibit a reversed current being generated once the voltage over the load is greater than the source[28][30].

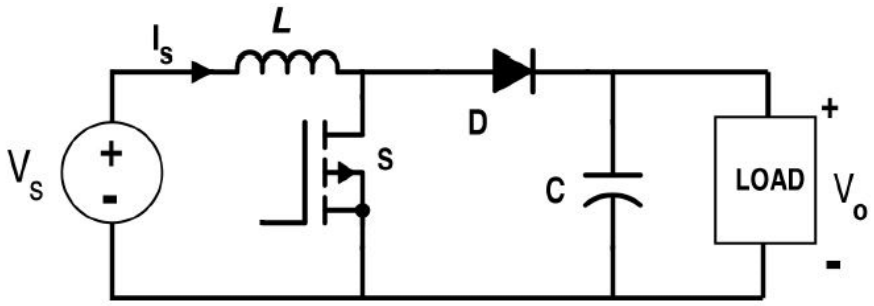

Figure 16: Circuit diagram of boost converter

2.3.3 Maximum Power Point Tracking

Two of the natural hinders of many energy harvesting technologies, and solar energy in particular, are the constant change of the amount of harvestable power and the fact that the conversion efficiency is low. It is also true that the current-voltage (IV) relationship and the power-voltage (PV) relationship are nonlinear for PV cells. Since the power output of the solar panel is ever changing, the maximum power output in relation to the voltage also changes. In figure 17 an IV curve (left) and a P-V curve (right) for a generic PV cell is shown. Maximum Power Point Tracking (MPPT) is an essential operation done in an EHS due to the importance of optimizing the sampling of available power. MPPT refers to the tracking of the point in the I-V curve that produces the maximum power output. A number of different MPPT techniques can be implemented in hardware to produce this effect. The different tracking algorithms vary in computation energy and accuracy and a compromise between the two aspect needs to be taken into consideration [24].

2.3.4 MPPT Algorithms

In order to track the point in the I-V curve that yields the maximum power output, different tracking algorithms can be used. As stated, the algorithms requires different amount of computing power,

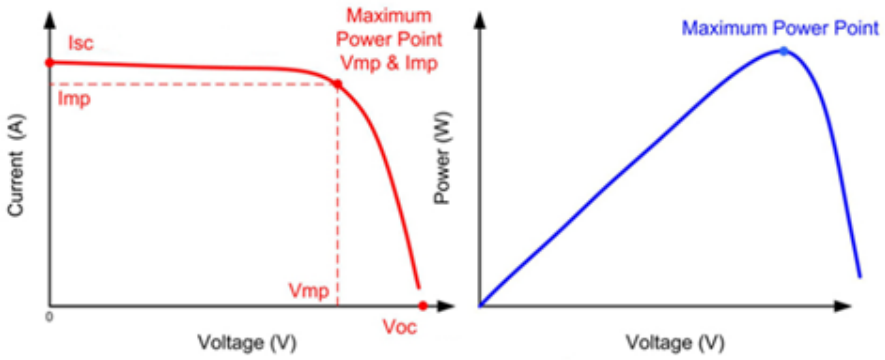

Figure 17: General I-V and P-V curve at STC conditions a 1000 W/m^2 irradiance

trading off in different accuracy of the MPPT operation. When working in a low power application, it is important that the algorithm used, is suitable for the task. In this section, the pros and cons of some of the different algorithms will be presented [24]. The working operations of two of them will be presented in a flow chart to show the different physical phenomena that can be used to achieve the MPPT.

Firstly, the differentiation between indirect tracking algorithms and direct tracking algorithms needs to be made. The indirect methods rely on assumptions and empirical data that hints to what the MPP is in certain conditions. An example is the fixed voltage methods, which assume the MPP is lower in summer than in winter and adjust the MPPT accordingly. Another example is the fractional open circuit voltage (FOCV) method, which makes the assumption that the MPP is a fixed fraction of the open circuit voltage. Both of these methods require less computation power and are easy to implement but lack in accuracy. For the FOCV method, it is also true that for the method to respond to changes in irradiance quickly, the OCV must be measured often. To do this, the PV cell must be momentarily removed during the measuring, which decreases the utilization of the PV output [24].

The direct tracking algorithms are often more sophisticated and accurate. Some of the most used direct tracking algorithms are based on the hill climbing concept. The hill climbing concept is a way to find peaks in curves by studying points along said curve. The goal of hill climbing, as the name suggests, is to go along a curve in a direction that yields higher and higher values until values start to decrease and a local maximum to the curve has been found. A common hill climbing technique is the Pertrube and Observe(PnO) algorithm. In this method, currents and voltages are measured from the PV cell and multiplied to obtain the power. These power values are then compared to previous measurements. If, for example one measurement value is called p1 and the other is called p2, assuming that p1 is measured at the voltage v1 and p2 is measured at the voltage v2, the following is true [21].

Assume:

$$v_1 < v_2 \; and \; p_1 < p_2 \tag{17}$$

This means that the MPP is to the right of the measured points. The perturbation will continue with higher values of v1 and v2 until the maximum is found . Assume:

$$v_1 < v_2 \; and \; p_1 > p_2 \tag{18}$$

This means that the MPP is to the right of the measured points. The perturbation will continue with

lower values of v1 and v2 until the maximum is found.

In the flow chart in figure 18, the general operation of the PnO is described.

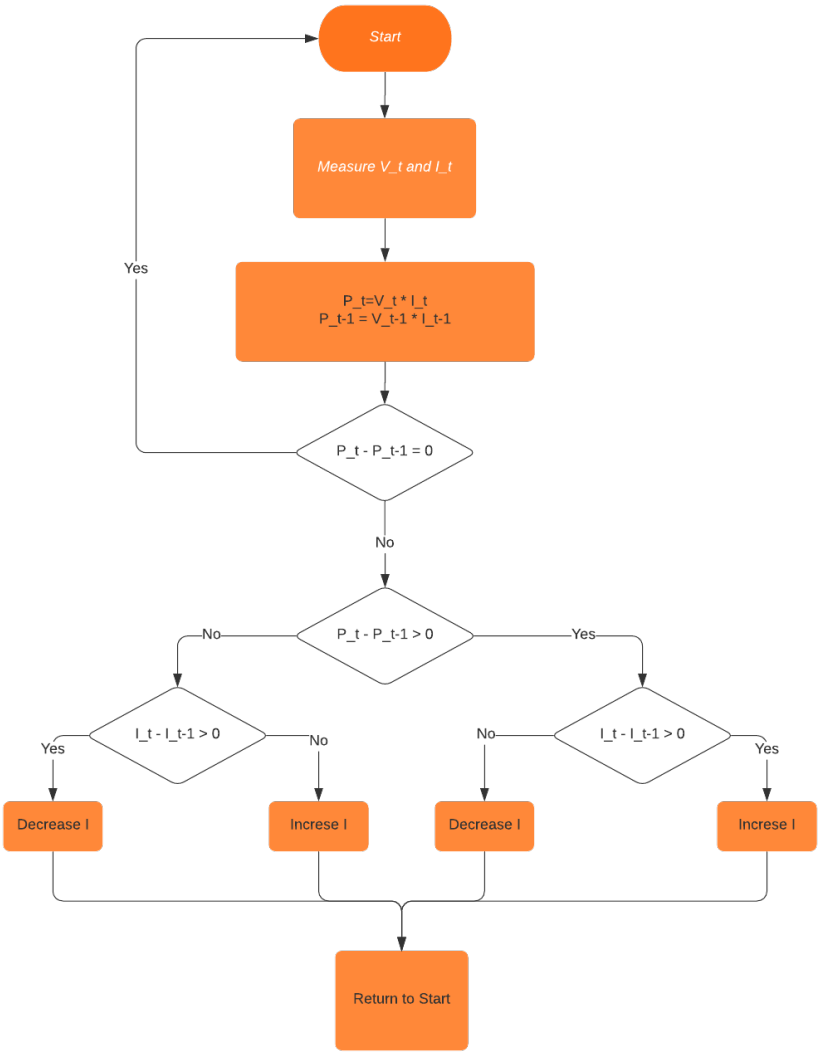

Figure 18: Flow chart of basic PnO operation

Another direct MPPT is the incremental conductance algorithm (ICA). This technique compares the instant conductance values I/V to the incremental conductance values $\Delta I/\Delta V$. This technique is able to find the MPP due to the fact that the P-V curve has a zero derivative at the MPP, meaning that the voltage and, therefore, conductance is not changing at this moment [21].

In the flow chart in figure 19, the general operation of the ICA is described.

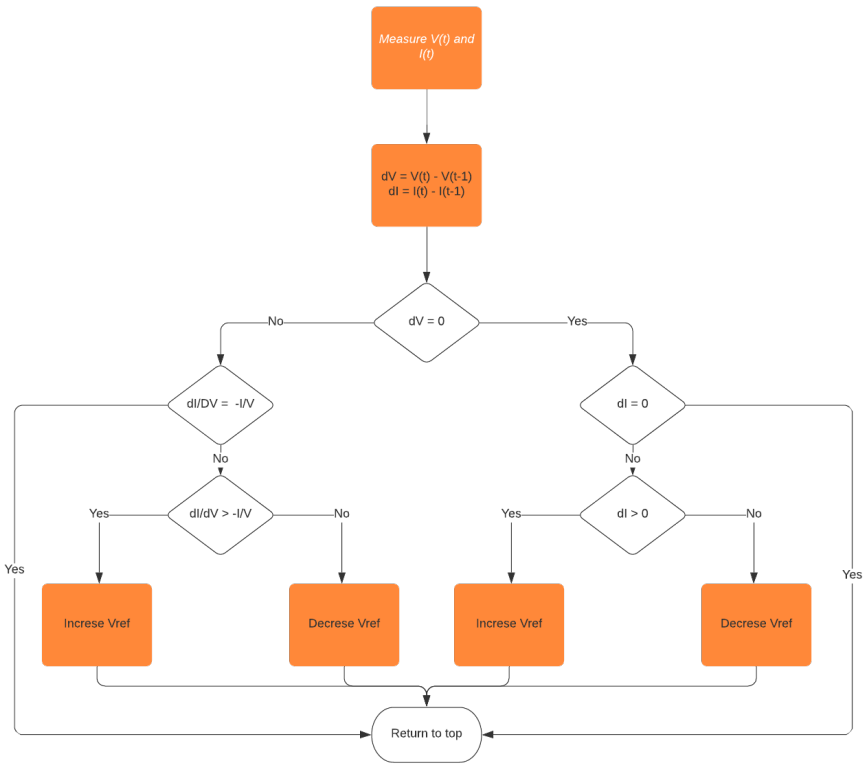

Figure 19: Flow chart of basic ICA operation

2.3.5 Energy Storage Units

Lithium-ion batteries has in recent years become the dominating technology in portable and wireless devices. Depending on the use case, a lithium battery has to be constructed accordingly. Trade offs in energy, power, charge cycles and environmental impact often dictates the battery's performance. However, the reason for these batteries popularity is due to their high gravimetric and volumetric energy density. The reason for the high energy density is its higher operating voltages resulting from the use of nonaqueous, water-free electrolytes in contrast to earlier battery technologies [17].

Supercapacitors are another type of energy storage often considered in energy harvesting systems. These units are in short just high capacitance capacitors, although, the working principles are somewhat different. Supercapacitors have some clear pros in comparison to other energy storage units, but also, some clear limitations. In comparison to lithium ion batteries, the energy density is much lower in terms of gravimetric energy density than that of lithium-ion batteries. On the other hand, the super capacitors are able to charge much faster under the right conditions. Supercapacitors can also be discharged without regards to discharge protection, meaning that a supercapacitor can be fully discharged compared to lithium ion batteries that should not be discharged beneath a certain voltage. Some limitations regarding supercapacitors exists however. One problem is their higher self discharge rate which negatively effects long term energy storage. Another problem is the output voltage loss experienced throughout their charge cycle compared to lithium-ion batteries, which output an almost constant voltage during its complete charge cycle [2].

In table 1 some key parameters are presented for supercapacitors and lithium ion batteries. The data

shown for supercapacitors is referred to electrical double layer capacitors (EDLC) as they are the most commonly used today [15].

Attribute	EDLC Supercapacitor	Lithium ion battery
Charge time [s]	1-10	600
Cycle life	1 000 000	500
Cell Voltage [V]	2.7	3.6
Specific Energy [Wh/kg]	3-5	250
Operating Temperature [degC]	-40 to 65	-20 to 60
Monthly self discharge [percent]	60	4

Table 1: Showing key performance parameters for supercapacitors and lithium ion batteries [15]

2.3.6 Development Kit for Energy Harvesting Performance Evaluation

A development kit has been provided by Verisure to use for the initial evaluation of the output performance of the OPV. This development kit logs many parameters, which will all be useful in order to analyze both the charging performance and the OPV performance. The development kit consists of one sensor device used for measuring all parameters and one raspberry pi that polls data from the sensor device via "bluethooth low energy" in set time intervals [7]. The parameters that the sensor can read and are analyzed in our experiments, are presented below in table 2.

Parameter	Description
LEH Current	Current sampled at the MPP of the OPV
LEH Voltage	Voltage sampled at the MPP of the OPV
SEC Current	Charging current of the seconday battery (rechargeable LI-ion battery)
SEC Voltage	Voltage over secondary battery (rechargeable LI-ion battery)
Illumination	Light intensity measured in lux from the lux meter on the sensor device
Temperature	Temperature measured inside of sensor device
Irradiance	Irradiance measured in W/m^2 from external irradiance meter

Table 2: Development kit parameters.

The development kit is based on an energy harvesting IC from Texas Instruments, model "bq25505". This energy harvesting chip takes care of the DC-DC conversion from the output of the OPV to the desired voltage needed to charge the secondary battery inside the sensor device. It also features a FOCV MPPT regulation configureable with external resistors. Besides this, the IC takes care of overcharge protection and discharge protection needed when charging a LI-ion battery. An external irradiance meter

was also provided so that the irradiance can be measured close to the active area of the OPV. This setup makes it possible to analyze both the charging performance of this specific EHS, but also the output performance of the OPV.

A CRON job on the raspberry pi is programmed to poll the sensor device once every minute to fetch information from all measurable parameters. This CRON job can be disabled and replaced with a shell scrip for example, in order to poll the sensor device at a smaller time interval. The script that runs in order to poll the sensor device takes approximately 5 seconds to complete restricting the resolution of the poll interval.

3 Component Evaluation

To optimally transfer energy from the output of the OPV to a potential energy storage, a few components are needed. This section presents how each component is evaluated and how the final components, used in the EHS, are selected.

3.1 Evaluation Process Description

In order to develop an efficient EHS, the evaluation in the working components, and the order of which they are evaluated is important to make good decisions regarding construction, construction materials and electrical components. Since the output performance of the OPV is the key factor for deciding the operational voltage and current range, it is important that this performance is evaluated and charted first. For this project, it was determined that the active area of the OPV panel was to be 55x53mm. Initially, the performance will be charted with an IV curve study.

A performance study of the OPV panel is then done to study how different factors, such as material, background colour, form factor and curve radius affect performance. This evaluation is done with comparability, and repeatability in mind. The tests are done indoors on a purpose built test bench that allows for the parameters to be studied.

In order to make the best use of the active area of the solar cell, the number of cells must also be defined, such that the charging output power from the IC is optimal. This means to choose the optimal number of cells to fit on the active area, adjusting the voltage output of the OPV, without sacrificing active area. The cells need to be separated for isolation purposes.

An outdoor data gathering of the light harvesting OPV will be conducted in order to get an understanding of how the indoor test and results translates to a real scenario. The outdoor logging also allows for more knowledge on what irradiance to expect in different lighting scenarios.

The results from the four evaluation procedures described above are all needed in order to make a good choice of electrical components. Specifically, the results from the tests are necessary to make a good choice of an energy harvesting IC, which will be the basis of the PCB. After the IC is selected, a battery type must also be selected before configuring the IC to work good with the whole system.

3.2 IV Curve Study

3.2.1 Background

In order to get an understanding of the performance of the OPV in terms of voltage and current output, producing IV-curves at different irradiance levels will yield valuable information. From the IV curves, the estimated voltage and power outputs will be charted and an estimated operating range will be determined. Since the OPV panel will be operational throughout the whole year, the energy harvesting system will have to endure the full range of irradience-levels that can be experienced. The IV curves will also give information on what the open circuit voltage, the short circuit current, and the maximum power point will be.

3.2.2 Method

The irradiance levels experienced in clear skies, uninhibited by clouds or fog are approximately $1000W/m^2$, corresponding to the irradiance level in the STC specifications. In STC, the voltage and power outputs are at their maximum and the absolute maximum ratings of the energy harvesting system can be chosen accordingly. The IV curve in STC has been provided by Verisures OPV manufacturer and is shown in fig 20.

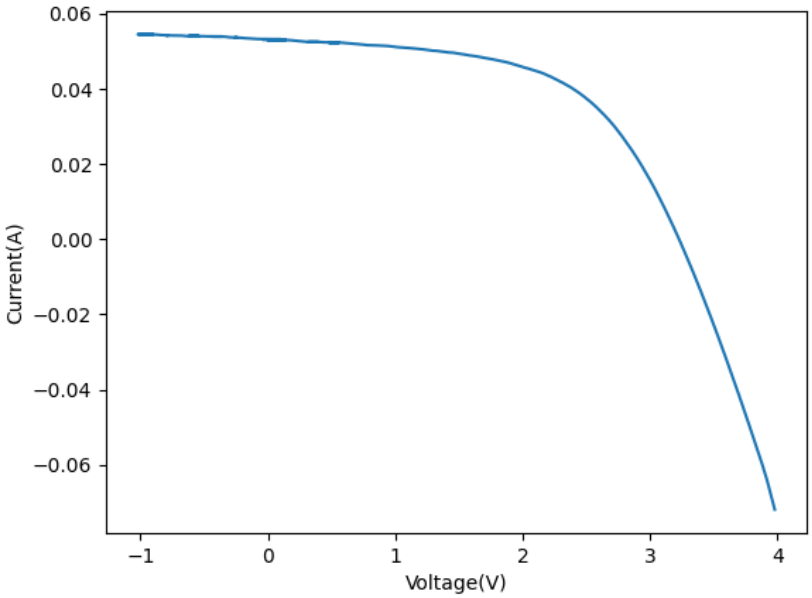

Figure 20: IV curve generated in standard test conditions.

Of equal importance is the OPV output performance for irradiance levels less than STC. This will give information on how the OPV performs in conditions much more likely to occur in the cell's everyday operation. The IV curves for $800W/m^2$ down to $200W/m^2$ will therefore be developed in $200W/m^2$ increments.

The IV curves were generated by connecting a variable resistor to the outputs of the OPV and measuring the current and voltage at the output of the OPV whilst varying the value of the resistance. The measurement setup is illustrated in figure 21

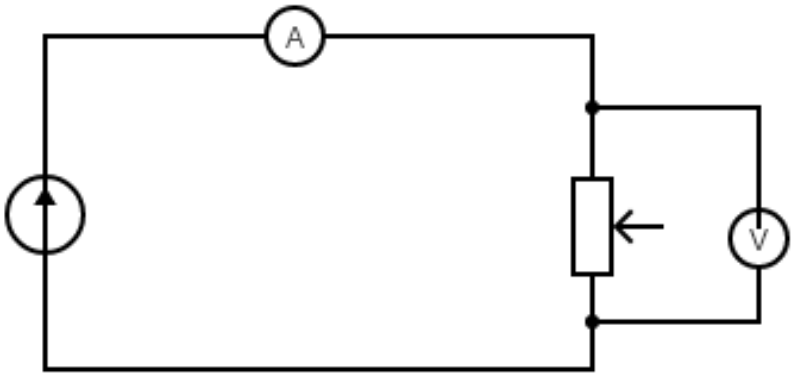

Figure 21: Circuit for generating IV curves

For all of the IV curves generated, the OPV was curved with a radius of 30mm as it is supposed to be in the final application. No cooling was provided for the cells as it was of interest to know how the OPV would perform in warmer climates with the sun naturally heating the panels.

To study the effects of photoactivation a first set of IV curves were made for the OPV panel before it had been exposed to any significant light intensity. A second IV curve was then generated after it had been exposed to a light intensity of 800 W/m^2 for 6 hours.

3.2.3 Results of IV Curve Study

The results of the IV curve study is presented below in figures 22 and 23. In both figures, the measured values making up the dotted lines were generated before the photoactivation process. The continuous lines shown in the graphs are made up of measured values after the photo activation process was done.

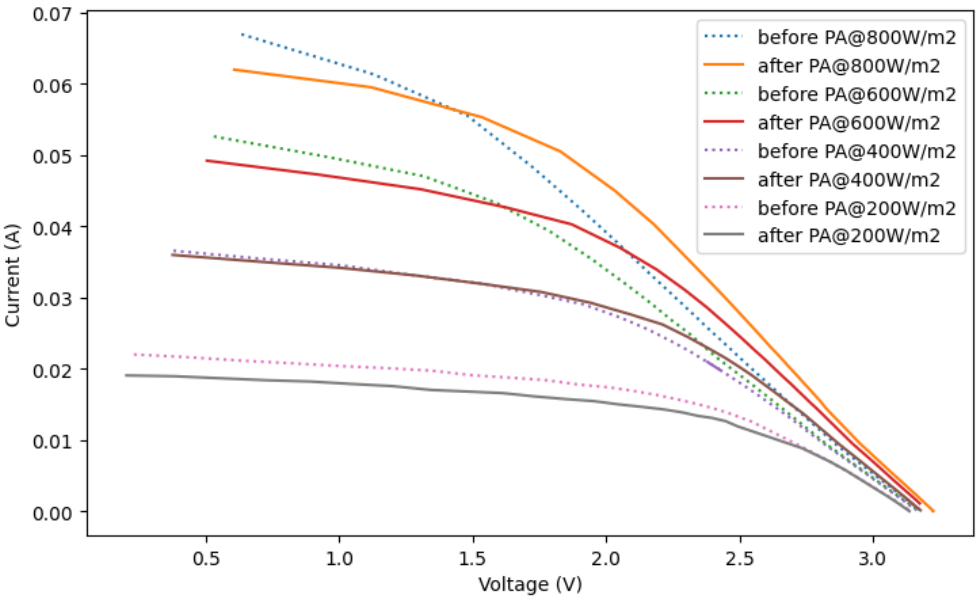

Figure 22: Current plotted against voltage for different irradiance levels

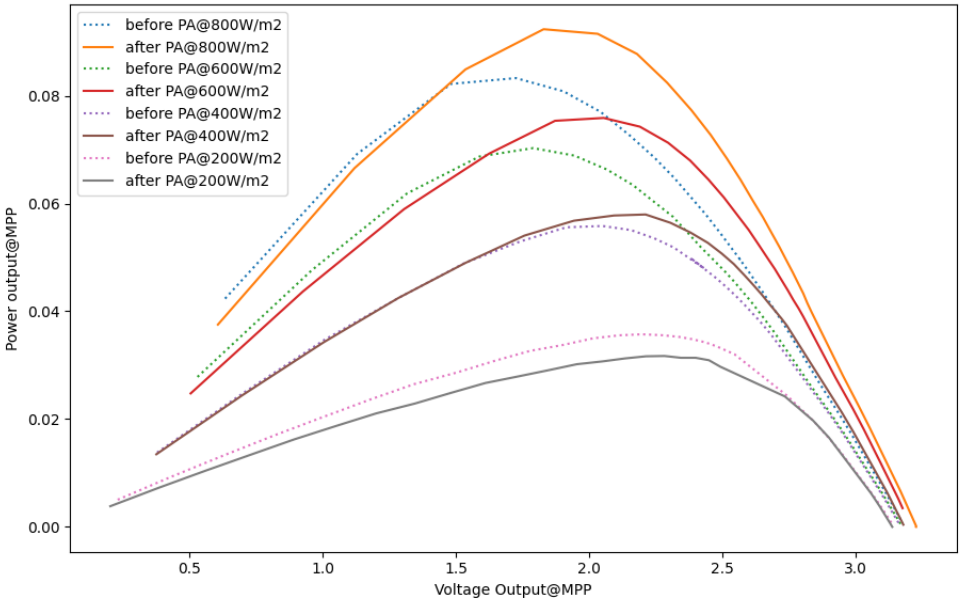

Figure 23: Power plotted against voltage for different irradiance levels

3.2.4 Discussion and Conclusions from IV Curve Study

When comparing the STC IV curve shown in figure 20, it is easily recognized that the curves differ. First of all the MPP from the STC IV curve is attained at 70% of the open circuit voltage. As stated before, the STC tests are done during very specific circumstances, with a light source that replicate the wave

Light Intensity (W/m^2)	**MPP (% of** V_{oc} **)**	V_{mpp} **(V)**	I_{mpp} **(A)**	P_{mpp} **(W)**
200(before PA)	0.70	2.1966	0.01627	0.0356
400(before PA)	0.64	2.0496	0.02724	0.0558
600(before PA)	0.56	1.7887	0.03929	0.0702
800(before PA)	0.54	1.724	0.0483	0.0832
200(after PA)	0.72	2.2816	0.0139	0.0317
400(after PA)	0.69	2.2107	0.02622	0.0579
600(after PA)	0.64	2.0534	0.03695	0.0758
800(after PA)	0.56	1.8281	0.05051	0.0923

Table 3: Results of IV curve study.

length spectrum of daylight, a light intensity of $1000W/m^2$, traveling through the atmosphere 1.5 times the vertical distance of it and at a temperature of 25 °C on the surface of the panel. The lamp used to get the results, presented in section 3.2.3, is commonly used to test PV panels but might not be the exact same that was used to generate the STC curve, this may introduce some source of error.

It is also noted that the irradiance meter used to determine the irradiance levels present at testing, uses a silicon based PV to sample a reference voltage that is translated to a irradiance level. This working principle will introduce some dependency of the silicon based PVs absorption spectrum, resulting in slightly different irradiance-level readings for different types of light sources. These irradiance meters are still used since the introduced error is assumed small. Pyranometers, which instead analyzes the whole range of irradiated wavelengths of the light source, give more exact readings but are too expensive, in comparison to the benefits of using them.

When analyzing the MPP of the different IV curves, two thing are noticed. Firstly, the MPP is decreased for higher irradiance levels and secondly, the MPP increases for the IV curves measured after the photoactivation. The reason for the MPP to decrease for higher irradiance levels is unclear, and the phenomenon is unexpected compared to how silicon PV cells behave. For higher irradiance levels, the open circuit voltage increases, and often the MPP of a PV cell output increases linearly [16]. When increasing the irradiadion levels from $200W/m^2$ to $800W/m^2$, the MPP for the provided cell instead decreased from 70% to 54% of its open circuit voltage before photoactivation and 72% to 56% after photoactivation, respectively. A possible cause for this is the temperature increase experienced as the irradiance increases. It is also noted that the internal resistance of the OPV increases for higher irradiance levels. In figure 22, this can be seen as the increase in voltage at the short circuit current point for higher irradiance levels. For the higher irradiance measurements it is also evident that both the shunt and series resistance have increased. This can bee seen as an increased slope at I_{sc} and V_{oc}. Since the exact composition of the OPV is unknown, the reason for an increased shunt and series resistance is not fully understood. This increase in resistance is however the reason for pushing the MPP to lower levels at higher irradiances. This phenomenon would suggest that the amount of power that can dissipate through

internal resistance in the OPV is disproportionately bigger for high irradiance exposures.

As mention above, it is also noted that the photoactivation process had a positive effect on the MPP of the OPV cell. This is easiest recognised when analyzing the power output from the OPV cell working at the MPP(P_{mpp}). For the irradiance levels 800, 600 and 400, P_{mpp} is 8% higher on average after photoactivation. It is assumed that a faulty measurement produced the result showing that the MPP is lower after photoactivation for the $200W/m^2$ irradiance level. This, since the area of the light pattern that exposes the OPV with $200W/m^2$ is small and depends on more accurate placement of the OPV to produce accurate results.

The results from this IV curve study will allow for valuable information when evaluating and configuring an energy harvesting IC. For instance, it is desired to sample the OPV panel at an MPP of 65% instead of 70% of the open circuit voltage as a safety measure, since the power decreases more rapidly to the right of the MPP.

3.3 Energy Harvesting Chip Evaluation

3.3.1 Background

Energy harvesting solutions for low energy applications are available from a number of different manufacturers. As presented in section 2.3.1 an energy harvesting solution meant for charging a battery must include a DC-DC converter and preferably a MPPT regulator. For the application at hand, energy harvesting solutions taking care of the DC-DC conversion and MPPT regulations are often packaged as Integrated Circuits (IC). A number of different ICs from different manufacturers are available too choose from, each displaying their own pros and cons. In order to maximize the overall efficiency of the energy harvesting system, the choice of IC is very important.

The three different IC chips considered in this project is the "Texas Instruments: bq25505", "E-Peas: AEM 10300" and "E-Peas: AEM 10941". These chips are very desireable to use since they include efficient DC-DC converters, handles the MPPT regulation and can be configured to handle overcharge and discharge protection.

3.3.2 Method

In order to evaluate the different chips the knowledge drawn from the IV curve study described in section 3.2 is used to make well based decisions regarding which IC to proceed with for further evaluation. The specifications of each IC must be carefully evaluated to match the operational output of the OPV that it is to be paired with. Below is the specification of the ICs properties that are to be evaluated,

An initial evaluation of the ICs can be done just by comparing the absolute maximum rating of each chip to the OPV output. This will potentially allow for identification of any ICs that can not operate with the given power output of the OPV. These ICs will in that case be ruled out and not included in the proceeding evaluations.

The ICs that are not ruled out in the initial evaluation will then be compared against each other in a decision matrix where each specification will be weighted according to its importance and a final selection of an IC will be made.

Specifications
Absolute Maximum Ratings
Operating Temperature
Recommended Operating Conditions
Cold Start Procedure
Charger Efficiency in STC conditions
Charger Efficiency in everyday conditions
Overcharge Protection Ability
Discharge Protection Ability
MPPT algorithm
MPPT poll time intervall
External BOM

Table 4: IC specifications to evaluate.

Importance of Different IC Specifications

A decision matrix will be used to make a final choice of IC chip based on how its specifications presented in table 4 suit the application at hand. Below, the different specifications are described and the attributes that are important for the application presented. The specifications will also be given a weight between 1 and 5 corresponding to its importance that will be used in the decision matrix.

Absolute Maximum Rating

These ratings determine the range of voltage, current and power inputs that the ICs can handle. They will not be used in the decision matrix as they will result in a definitive exclusion of an IC if the OPV inputs a voltage or current that exceeds the ratings.

Cold Start Procedure

The cold start procedure of the ICs determines at what voltage/power input from the OPV the IC will initiate its start procedure from being in idle. Since working with low power applications, the cold start procedure is desired to have as low of a cold start voltage/power as possible for the IC to be active in low light environments as well. It is weighted **1** since the attribute only has an impact in very low light conditions.

Charger Efficiency in STC conditions

The DC-DC inverters integrated in the ICs are dependant of the input power from the OPV panel as well as the voltage level of the battery that they are charging. It is desirable that the efficiency is kept high even in STC conditions since the application is to be used in a variety of light conditions, even though

it is rare for the application to experience STC conditions. The attribute is weighted **4** since a majority of the energy harvesting systems losses are from the DC-DC inverter. The efficiency of the of the ICs in STC conditions will be determined based on the results of the IV curve study presented in section 3.2.3.

Charger Efficiency in Everyday Conditions $(200-400W/m^2)$

As mentioned above the DC-DC inverters efficiency will have a big impact on the total energy harvesting system's efficiency. This attribute is weighted **5** since the application is more likely to experience irradiation levels of $200-400W/m^2$. The efficiency of the ICs in everyday conditions will be determined based on the results of the IV curve study presented in section 3.2.3.

Overcharge Protection Ability & Discharge Protection Ability

Since lithium ion batteries take damage from being charged when containing its rated energy maximum and discharged when containing its rated energy minimum, it is important to not let any charging happen when the energy maximum is surpassed. It is also important to not draw any current from the battery when it is empty. The final application will consist of a battery that has its own overcharge and discharge protection making additional overcharge protection redundant. For testing and prototyping, the overcharge and discharge protection ability might still be useful if, for example, testing the abilities of the energy harvesting system with low capacity batteries to study the complete charge cycle. The overcharge protection and discharge protection ability is weighted **1**, respectively, because of the redundancy in the final application.

MPPT Algorithm Precision

In section 3.2.3 it is discovered that the MPP of the provided OPV shifts significantly under different irradiance exposures. It is therefore considered important that the MPPT regulation is efficient in finding the MPP. Of equal importance as finding the MPP is that the energy consumption during the MPPT procedure is kept low. This makes some MPP algorithms more suitable than others. The weight of this attribute is set at **5** since the OPV panel operating at the MPP is crucial for a high power output.

MPPT Poll Time Interval

The ICs can have different ways of implementing the time between the execution of the MPPT calculations. It is preferred that this time is configurable as a low poll time interval can adjust to changes in working conditions better. The trade-off however, is the energy spent on the MPPT calculations. The cut off point will be dependant on the total energy production of the energy harvesting system. This attribute is weighted **3** because of the importance of being able to adjust the poll time based on the expected power output.

External BOM

The ICs do need additional passive components in order to configure them for suitable operation, when implementing them on a PCB. It is desired that the BOM is kept small in order to decrease PCB size and ease the implementation of the PCB into the physical application.

3.3.3 Results of Energy Harvesting Chip Evaluation

Absolute Maximum Ratings

In table 5 the absolute maximum ratings of the ICs are presented [31][10][9].

	E-Peas 10300	E-Peas 10941	TI
Absolute Maximum Voltage	4.5V	5	5.5V
Absolute Maximum Current	–	110mA	90mA
Absolute Maximum Power	–	550mW	510mW
Battery Voltage Range	3-4.05	2.2-4.5V	2-5.5V

Table 5: IC absolute maximum ratings.

In the STC curve provided from armour seen in figure 20 it can bee seen that P_{max} is 92mW. The "E-peas: AEM 10300" chip does not present any power limitation in its data sheet and it is assumed to be able to handle the OPV panel output. All ICs will therefore proceed for further evaluation.

IC Efficiency Estimations

All specifications of the ICs that are to be evaluated are easily found when consulting their respective data-sheets, except the efficiency of the IC at STC conditions and everyday conditions. In order to specify this, it is necessary to refer to table 3, section 3.2.3, where the power output from the OPV can be found for $200W/m^2$, $400W/m^2$ and $1000W/m^2$, respectively. It is assumed that the panels will operate after the photoactivation process has been completed and the values from table 3 can be retrieved accordingly.

For irradiance levels of $200W/m^2$, the panel outputs 2.28V@13.9mA. At $400W/m^2$ the panel outputs 2.21V@26mA and at $1000W/m^2$, the panel outputs 2.24V@55mA. These working conditions can then be compared to the efficiency graphs in the respective data sheets. The graphs can be found in figures 24, 25 and 26 below.

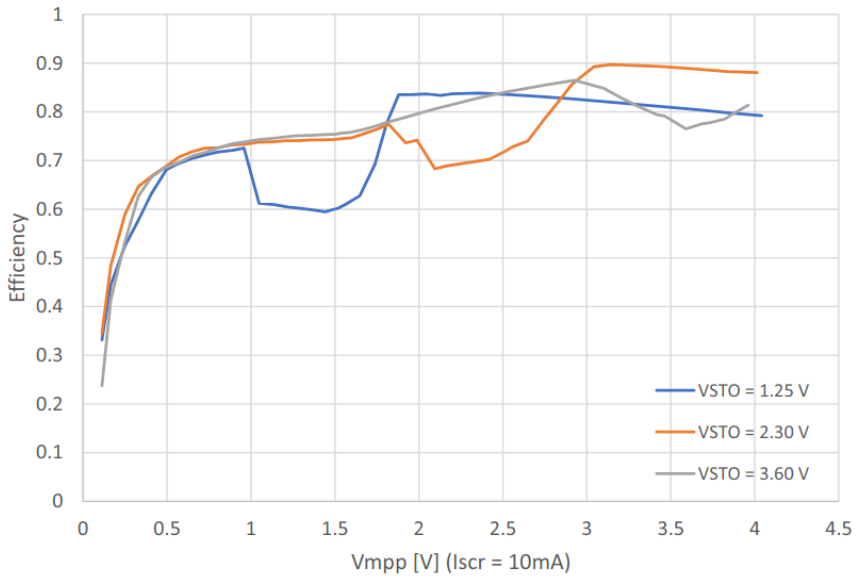

Figure 24: Graph showing the efficiency as a function of the AEM 10300 input operational voltage [10]

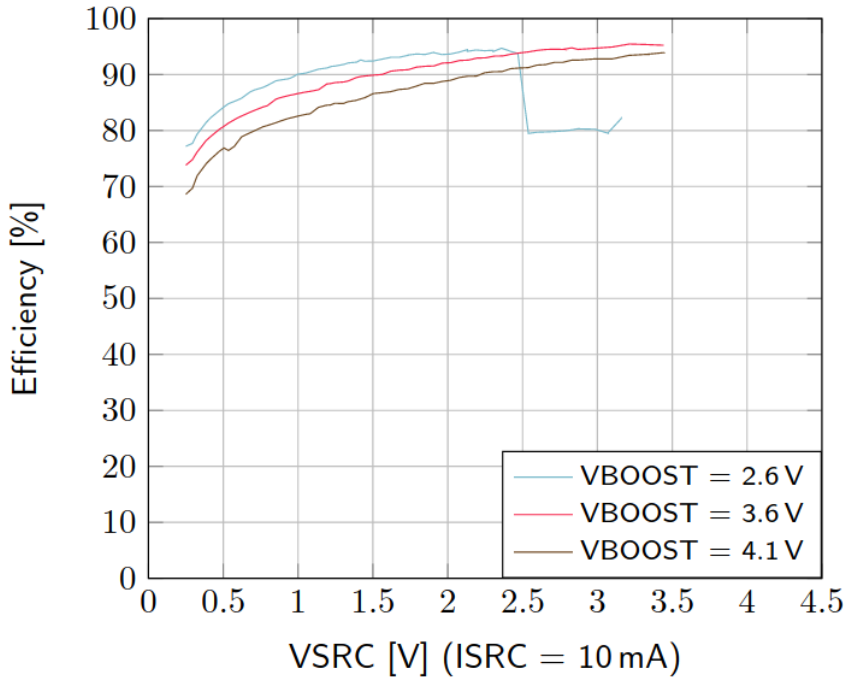

Figure 25: Graph showing the efficiency as a function of the AEM 10941 input operational voltage [9]

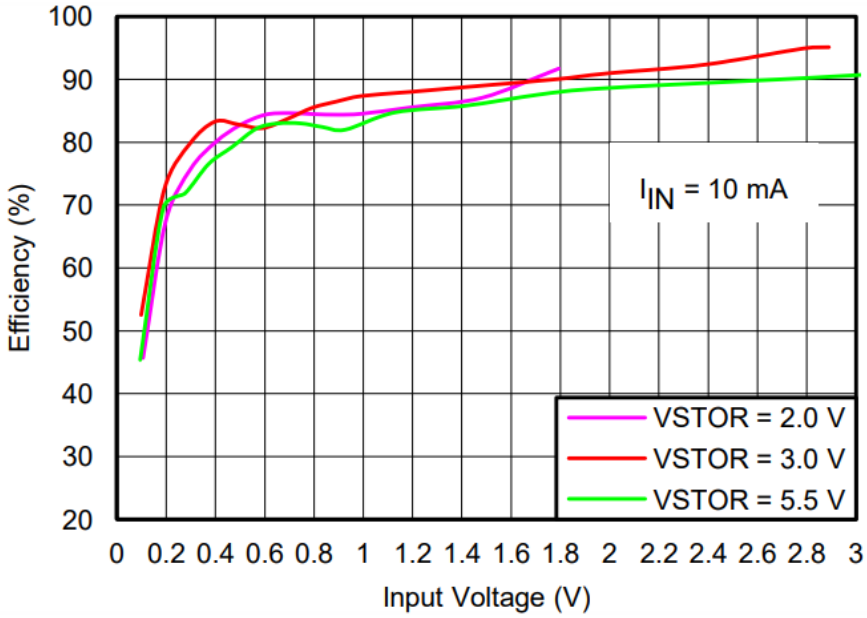

Figure 26: Graph showing the efficiency as a function of the BQ25505 input operational voltage [31]

From the graphs above, the efficiency of the IC chips in relation to the relevant irradiance levels is presented in table 6.

Irradiance (W/m^2)	**AEM10300 efficiency (%)**	**AEM10491 efficiency (%)**	**bq25505 efficiency (%)**
200	82	93	92
400	81	92	91
STC Conditions	82	93	92

Table 6: IC efficiency in relation to OPV output.

For the OPV panel, the desired MPP sampling setting is 65% of the open circuit voltage when using the FOCV sampling method. In figure 27, the power output of the panel is plotted against different irradiance levels when sampled at the MPP closest to 65% for each IC.

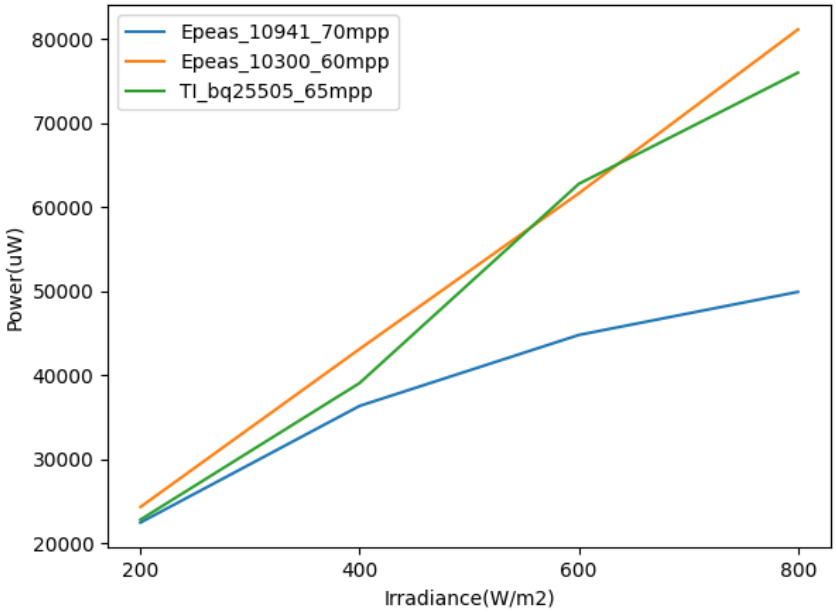

Figure 27: Graph showing the power output for the different chips set at different MPP sampling settings

Specifications	**Epeas AEM10300**	**Epeas AEM10491**	**TI bq25505**
Cold Start Procedure Conditions	275mV@3μW	380mV@3μW	600mV@15μW
Charger Efficiency in STC conditions	82	93	92
Charger Efficiency in everyday conditions	81-82	92-93	91-92
Overcharge Protection Regulation	Pin Configurable	Pin Configurable	Voltage Divider Regulation
Discharge Protection Ability	Pin Configurable	Pin Configurable	Voltage Divider Regulation
MPPT algorithm	FOCV@60-90%	FOCV@70-90%	FOCV@50-80%
MPPT poll time Interval	280ms-71s	5s	16s
External BOM	3 pieces	7 pieces	12+ pieces

Table 7: IC specifications [10][9][31].

Decision Matrix

From table 8, it is decided that the Texas Instruments bq25505 IC will be integrated into the energy harvesting system. The different IC chips have been scored relative to how each IC comply with each specification on a scale of 1 - 10.

3.3.4 Discussion and Conclusions of Energy Harvesting Chip Evaluation

The bq25505 IC was ultimately chosen to be implemented into a complete energy harvesting system. This since it scored best in the decision matrix. However, the IC does come with some drawbacks for

Specifications	Weight	Epeas AEM10300	Epeas AEM10491	TI bq25505
Cold Start Procedure Conditions	1	8	6	3
Charger Efficiency in STC conditions	4	6	9	8
Charger Efficiency in everyday conditions	5	6	9	8
Overcharge Protection	1	3	3	6
Discharge Protection	1	3	3	6
MPPT algorithm	5	8	3	8
MPPT poll time Interval	3	10	7	5
External BOM	3	10	7	5
Total Points		138	129	157

Table 8: Decision Matrix.

this implementation. For example, the large BOM needed to implement the IC onto a PCB introduces some limitations on the smallest physical size the PCB can have. An IC with a minimal BOM might for instance make it possible to implement it directly into the casing of a battery, avoiding electrical components in the medium between OPV and battery.

It is also noticed that all of the contenders in the decision matrix use a FOCV method to determine the MPP of the OPV. However, in section 3.2.3 it is presented that the MPP of the provided OPV is shifting in regards to the OCV for difference irradiance exposures. This would suggest that the best possible MPPT algorithm to use would be a direct method like the PnO or ICA methods described in section 2.3.4. Such algorithms would ensure that the OPV is working at the correct MPP.

It is noted, that when comparing the results in figure 27, the sampled input power of the OPV increases almost linearly for the "bq25505" and "AEM10300", which are working at an MPP of 65 and 60 % of the OCV, respectively. The AEM10941 is instead working at an MPP of 70 % of the OCV and a decrease in power, in relation to the bq25505 and AEM10300, can be seen as the irradiance levels increase. This is also a result of the MPP shifting to lower voltages for higher irradiance levels.

3.4 Indoor OPV Performance Test

3.4.1 Background

In order to test some important parameters of the the OPV and how it can be installed in its immediate surrounding, a set of indoor tests were defined. These tests can act as the basis of future design decisions and will indicate that the MPPT is sampling at a optimal FOCV as well as providing general knowledge on how the OPV works in conjunction with an EHS. The tests were conducted in a laboratory environment at LTH.

3.4.2 Method

In order to have reproducible, comparative and reliable tests of the OPV performance under different conditions a test bench meant for exploring the impact of the OPVs' physical parameters has been developed. The test bench is based on a full spectrum sulfuric plasma lamp, a rig that controls a rotating axis spinning 180 degrees in 30 minutes and several mounting adapters to install the OPV on. In all tests, the OPV panel will sit in parallel to the the rotating axis with the lamp directly above so that the incident light is perpendicular to the axis. The angle of the rotating axis can be changed however, so that the angle relative to the incident light changes. One test cycle conducted on the workbench is described below. From this test, the OPV power output can be measured with respect to a specific angle of the incident light.

Figure 28: Lamp and test bench

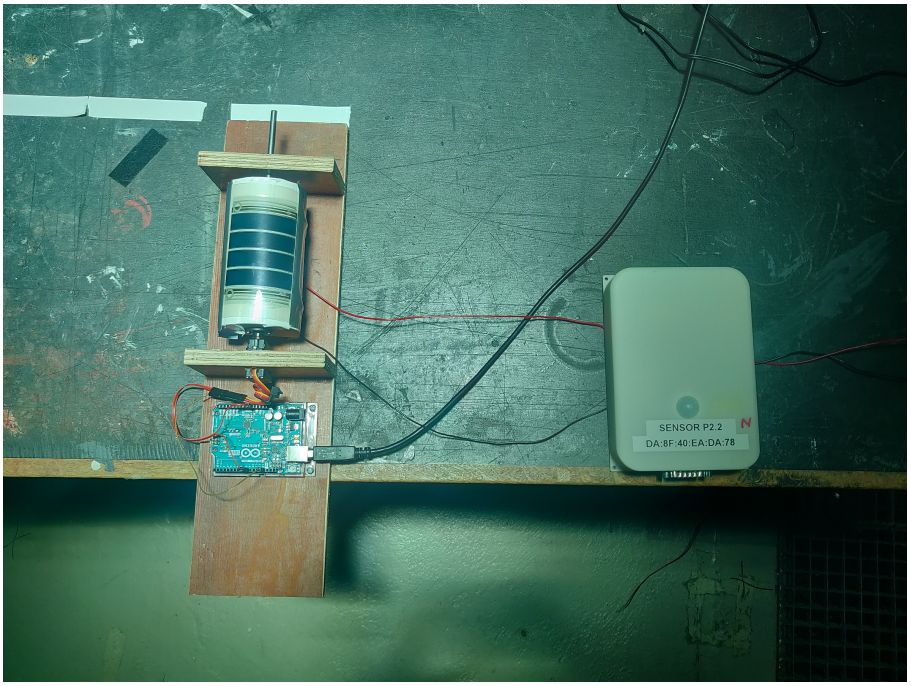

Figure 29: Test bench

- OPV will rotate on an axis. 180 degrees in 30 minutes.
- Measurements will be done every 5 seconds using the provided devkit.
- Measurements will be logged in a .csv file for later analysis.
- Irradiance will be fixed for the duration of the cycle.

The design parameters to be studied are the following:

- Background color/material.
- OPV surface radius.
- Partial shadowing.
- MPP performance.
- Effects of external cover lens.
- Temperature.

Background color/material will be studied by recording a test cycle on the test bench while a specific background color is applied behind the OPV. The background materials to be studied are white plastic tape, black plastic tape and an aluminum foil sheet covered by transparent tape. The best performing background material will be used for all further tests.

OPV surface radius Since irradiance levels will not make an impact on how different forms affect the power output only one irradiance level is used during the tests. Cylinders with a 30 and 60 mm radius and finally a flat rectangle will be used to explore various surface radii.

Partial shading will be tested by partially covering the OPV cell with reflective tape horizontally and

vertically. The cells will be tested when vertically covered so that 1/3 and 2/3 of the active area is covered. In an independant test the cells will then be tested when horizontally covered so that 1/4, 2/4 and 3/4 of the cell is covered, covering one additional cell each test. The change in performance will be recorded.

MPP performance is evaluated by comparing power output with a MPP set at 65 % and then 80 %. Irradiance level will have a big impact on how the OPV perform at different MPP and therefore testing will be done at 200, 400, 600 and 800 W/m^2.

A **Temperature** test is done to study the effect of OPV surface temperature in relation to the OPV power output. This is done by situating a room temperature OPV under the sulfur plasma lamp at $800W/m^2$ and taking note of the power output and surface temperature until no significant change can be seen.

The effect of different **OPV surface radii** during a test cycle described in section 3.4.2 is conducted. This is done by recording the power output from the OPV during the test cycle with a white background.

A **Cover lens** to protect the OPV for outdoor use can be needed. The OPV used in this rapport is somewhat weather resistant but if implemented for outdoor use, a cover lens will most likely have to be used. There is a lot of different design possibilities with a potential lens but the ones explored in this report will be thickness and percentage of color pigment. The lenses studied in this rapport is made of polycarbonate (PC). Color pigment is mainly be used to serve aesthetic purposes, such as a desired color of the lens. Evaluation will first be done with a transparency test using a light source and a pyranometer to determine the transparency of the lens.

Lastly an artificial UV-ageing test will be done with the clear lenses. It will span over 10 days simulating 30 days of solar radiation.

3.4.3 Results

Results from background color tests

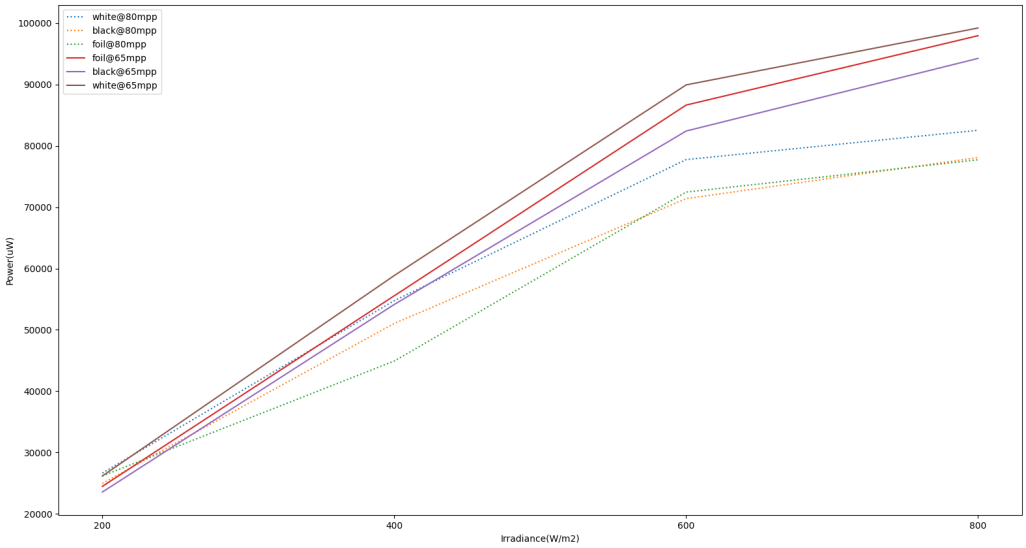

Figure 30: Power output for different MPP percentage.

Results from temperature tests

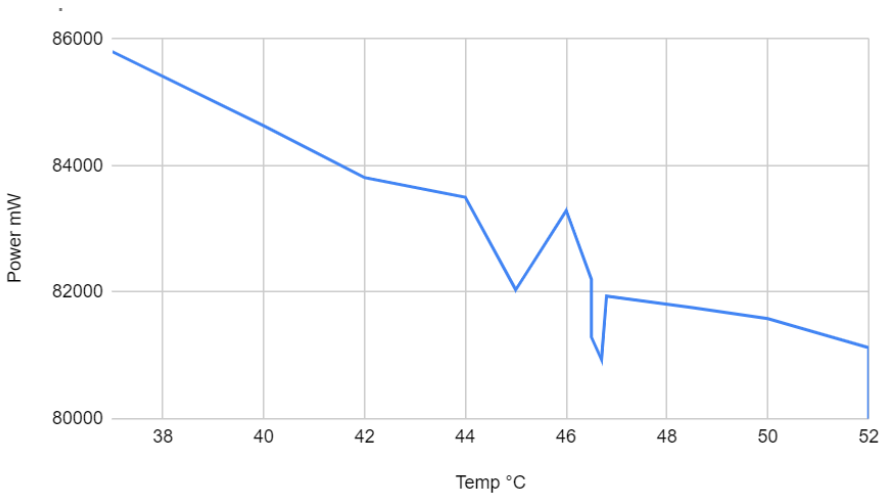

Figure 31: Power output at MPP 65% percent plotted against increasing OPV surface temperatures.

Results from cover lens tests

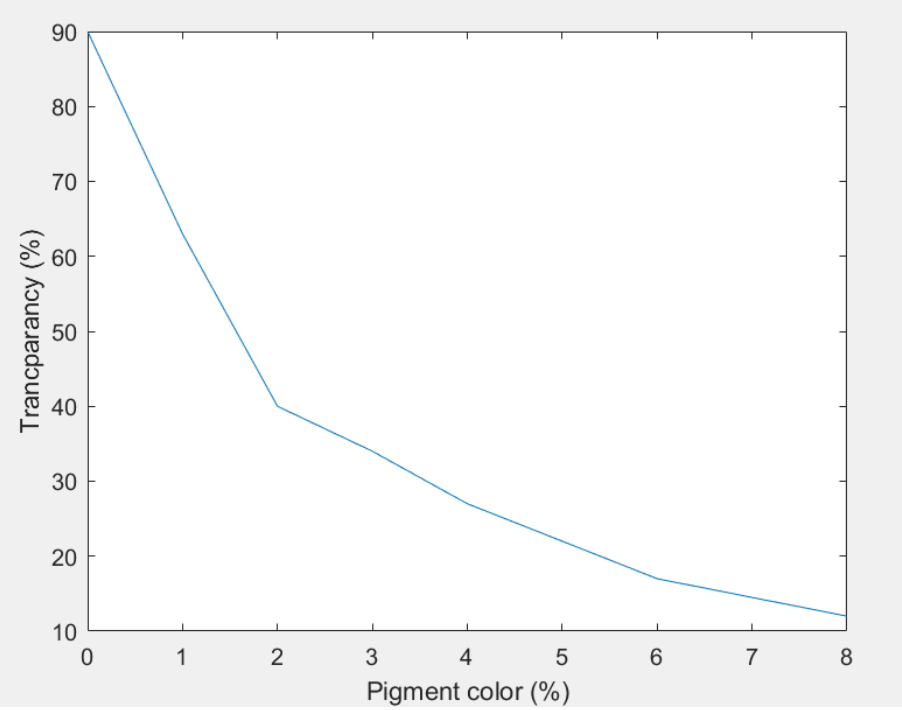

Figure 32: Correlation between color pigment and transparency

Pigment %	Transparency %
0	90
1	63
2	40
3	34
4	27
6	17
8	12

Table 9: Percentage of pigment in the lens and percentage of light let trough the lens.

Results from OPV surface radii tests

OPV surface radius(mm)	Mean Power
Flat	62.3
30	64.7
60	62.7

Table 10: Power outputs at different OPV surface radii.

3.4.4 Discussion and Conclusion on Indoor OPV Testing

During testing it should be noted that only 10% of the incident light originating from the light source goes through the OPV. This makes the difference in OPV power output in combination with different background colors, relatively small. The results presented in figure 30 shows that there is no color that outperforms the others in all irradiance levels, but using a white background often outperform the others. An explanation for this is that the black color absorbs more energy from the incident light resulting in less energy bouncing back and hitting the OPV from the backside. Surprisingly, the white background color also outperformed the aluminum foil + transparent plastic tape background. This is surprising since it was assumed that the aluminum would reflect the incident light better then the white plastic tape. The reduction in reflected light might be the result of a significant amount of energy being dissipated when transferring through the transparent plastic tape.

Regarding the MPP performance sampled at different FOCV, also presented in figure 30, it is shown that the suspected increase in power is achieved when sampling at a FOCV of 65% instead of 80%. This is in line with the results from the IV curve study presented in figure 3.2.3.

In the results of the temperature test shown in figure 31, a 7 % decrease was seen over 14°C. This means that the OPV loses about 0.5 % of the original power per degree.

Regarding the results from the cover lens tests presented in figure 32, the relation between transparency and pigment percentage can be understood. It can clearly be seen that the curve is exponential and that a small amount of black pigment in the cover lens will lead to a big decrease in OPV output power.

The studied OPV module consists of 4 cells connected in series. In figure 32 it is shown that shading cells lengthwise result in a power loss equal to the percentage of cell area covered. If one cell has 20 % of its area shaded the whole OPV module will produce 20 % less power. If you shade all 4 cells 20 % lengthwise the power production will still only decrease by the same as one cell being shaded. A complete black out of a cell horizontally will eliminate the power output completely. No power will be produced since electrons can not flow in the shaded cell that is connected in series to the others.

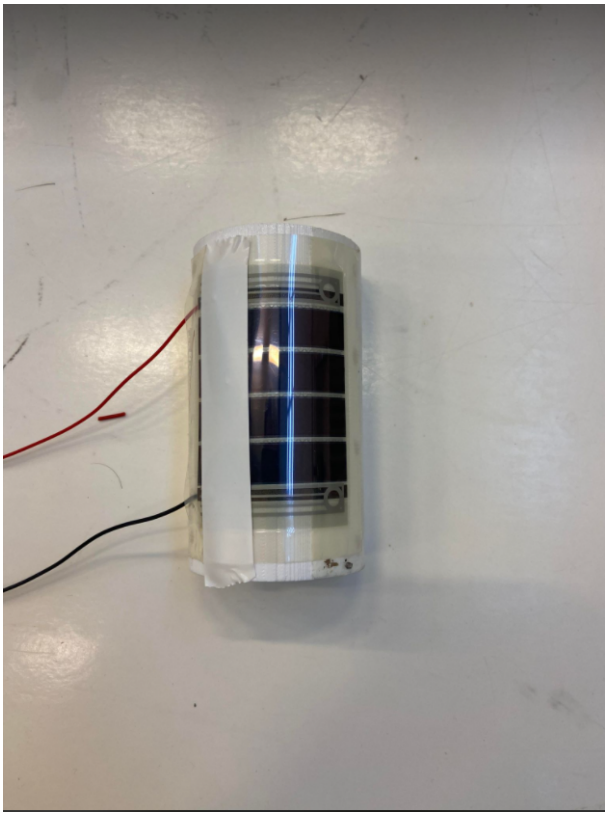

Figure 33: Shading of the opv module resulting in about a 20 % loss of power

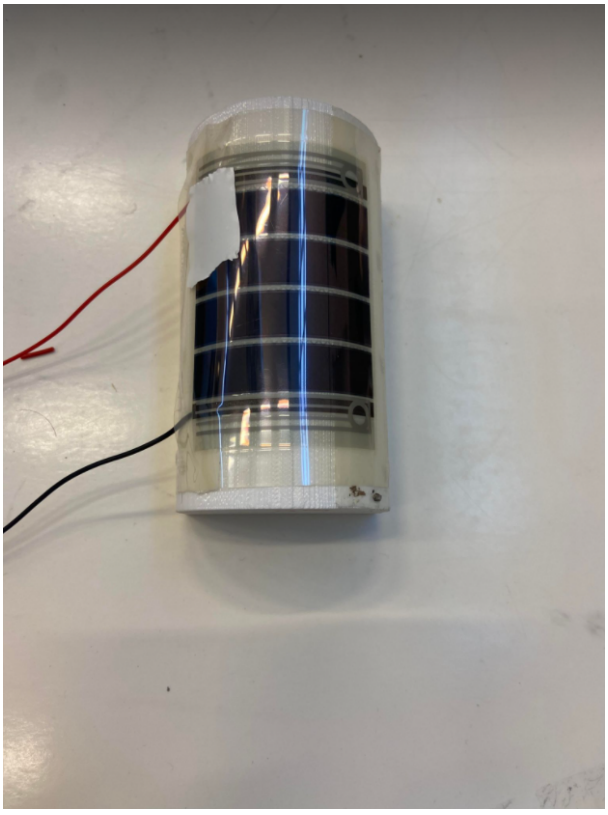

Figure 34: Shading of the opv module resulting in about a 20 % loss of power

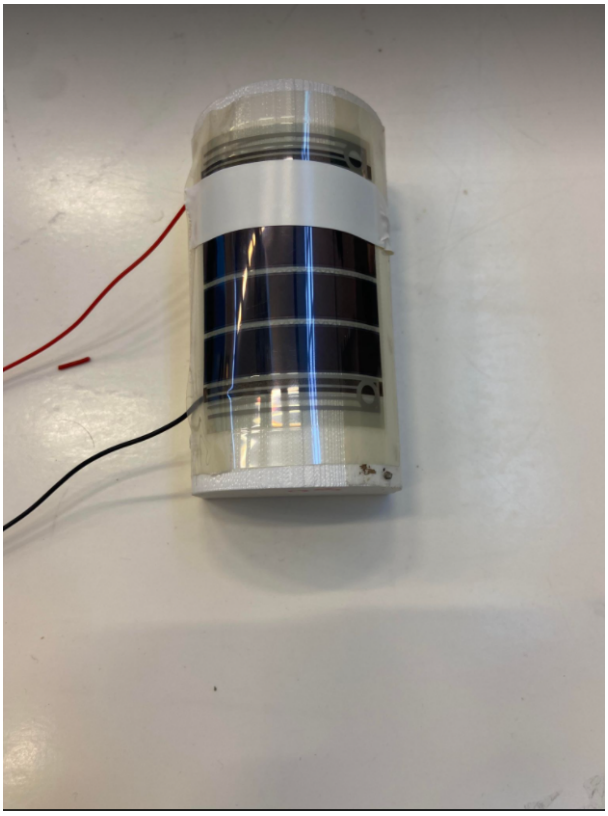

Figure 35: Shading of the opv module resulting in a 100 % loss of power

When comparing different OPV surface radii, it is noted that the 60mm radius performs best in terms of its mean value during one test cycle. This implies, that for the way this test is conducted, there seems to be an optimal radius for maximising the energy harvesting, somewhere between a infinity(flat) and 30 mm surface radii.

A direct relation between transparency and power can be seen in the results, meaning that 90 % transparency will reduce the power output by 10 % and so on. If a pigment % is desired over 8 % it will not significantly affect the transparency. Therefore no testing was done with pigment % higher than this.

A cover lens will have an extremely detrimental impact on OPV performance. Tinted lenses are especially bad and might be as bad as placing the OPV in constant shadow instead of direct sun. The main reason for using tinted lenses is as mentioned before aesthetics. If this is not a priority a clear lens is a better option. It was also seen that UV-ageing has an insignificant effect on transparency.

3.5 Outdoor OPV Performance Test

3.5.1 Background

The intention with the outdoor testing and data logging is to get an understanding of how the OPV panels behave in real world scenarios. The orientation of the OPV panels compared to incoming sunlight and the OPV output power will be studied, and the panels behaviour to diffused sunlight will also be recorded from the OPVs situated in shade. Effects such as partial shadowing, the impact of different angles of the

incident light and the effect of facing the OPV in certain directions will be captured in a very realistic setting. Ideally, this kind of data gathering should be conducted all year round to study the performance during all seasons, but due to time constraints, the data gathering will only be able to capture fall and winter data. The testing will occur in as many different weather conditions as possible except heavy rain and harsh winds.

3.5.2 Method

For the outdoor testing a portable testing rig shown in figure **??** is used. This rig has four mounting-faces pointing towards north, south, east and west. The panels will be mounted with a zenith angle set at 90°. External irradiance sensors will also be mounted on the same plane as the OPV panels so that the data gathered from the OPV panels can be compared to the irradiance levels present. Each OPV and irradiance-meter will be connected to a development kit to capture the relevant data. Since the effect of different MPP settings is of interest, cells will be mounted with 65% and 80% FOCV sampling. Only the south and north facing mounting-panels will be occupied by OPV cells since this test does not aim to suggest a yearly energy harvesting potential, but rather to confirm the MPP to be set correctly given the most optimal (south) and least optimal (north) directions. It also gives good insight in how irradiance levels change throughout a day.

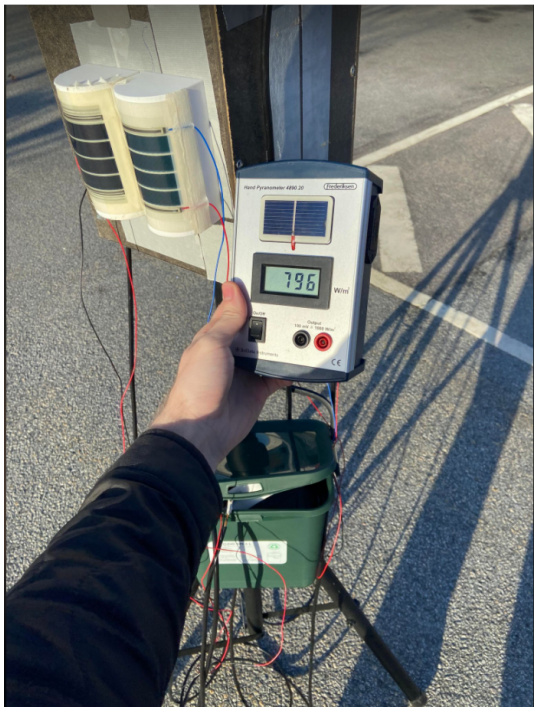

Figure 36: Outdoor testing with MPP sampling (FOCV) at 65 and 80 %

3.5.3 Results

Outdoor conditions: Mix of clouds and sunny sky 13 degrees °C. Location: Lund, Sweden.

Facing south:

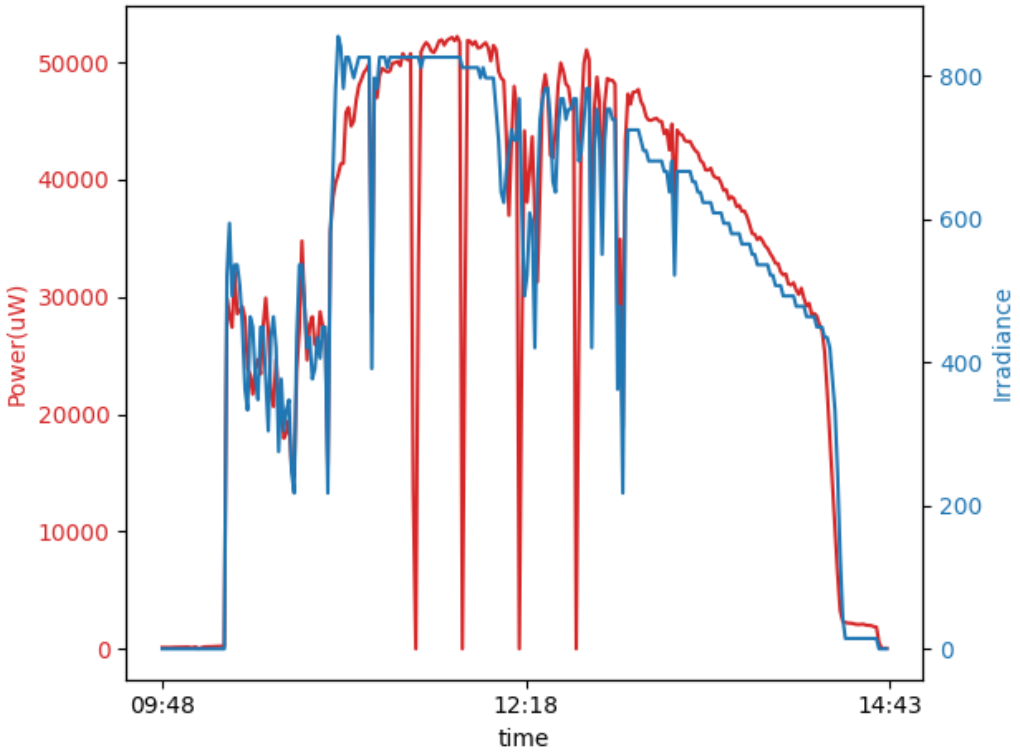

Figure 37: MPP sampling (FOCV) set at 80%. South facing

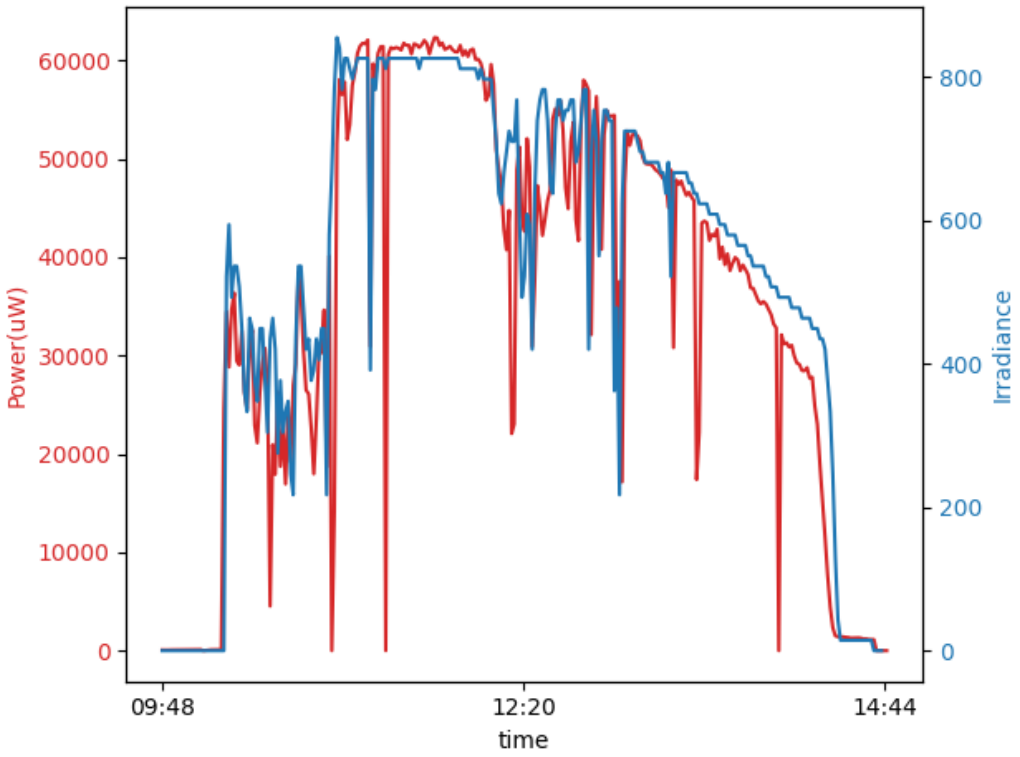

Figure 38: MPP sampling (FOCV) set at 65%. South facing

Facing north:

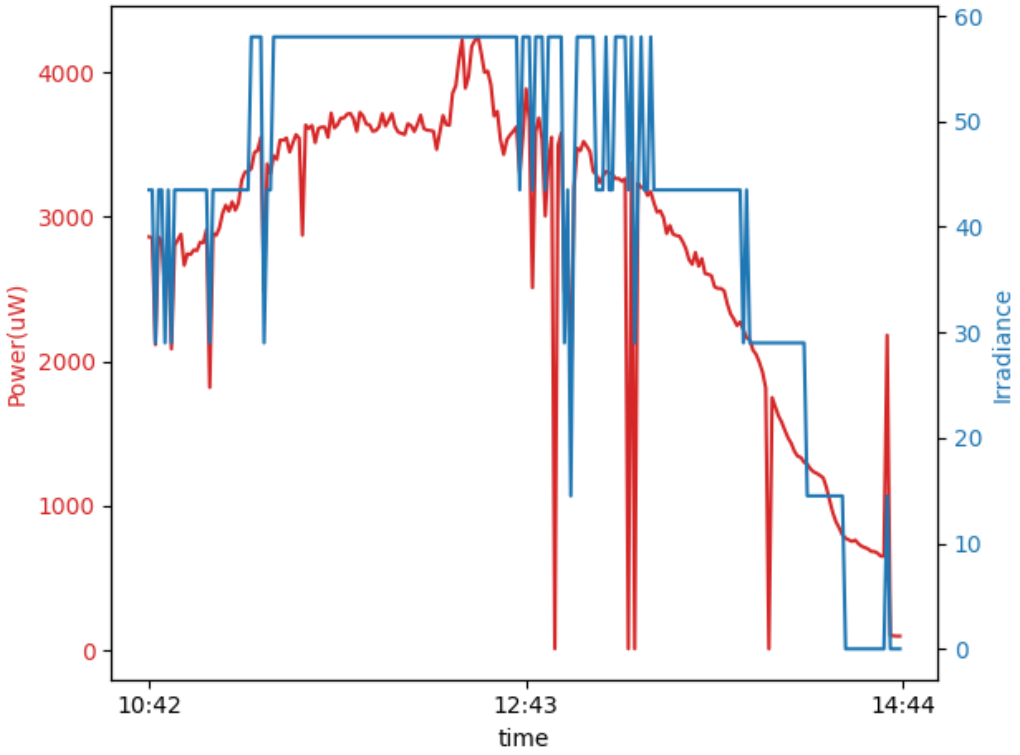

Figure 39: MPP sampling (FOCV) set at 65%. North facing.

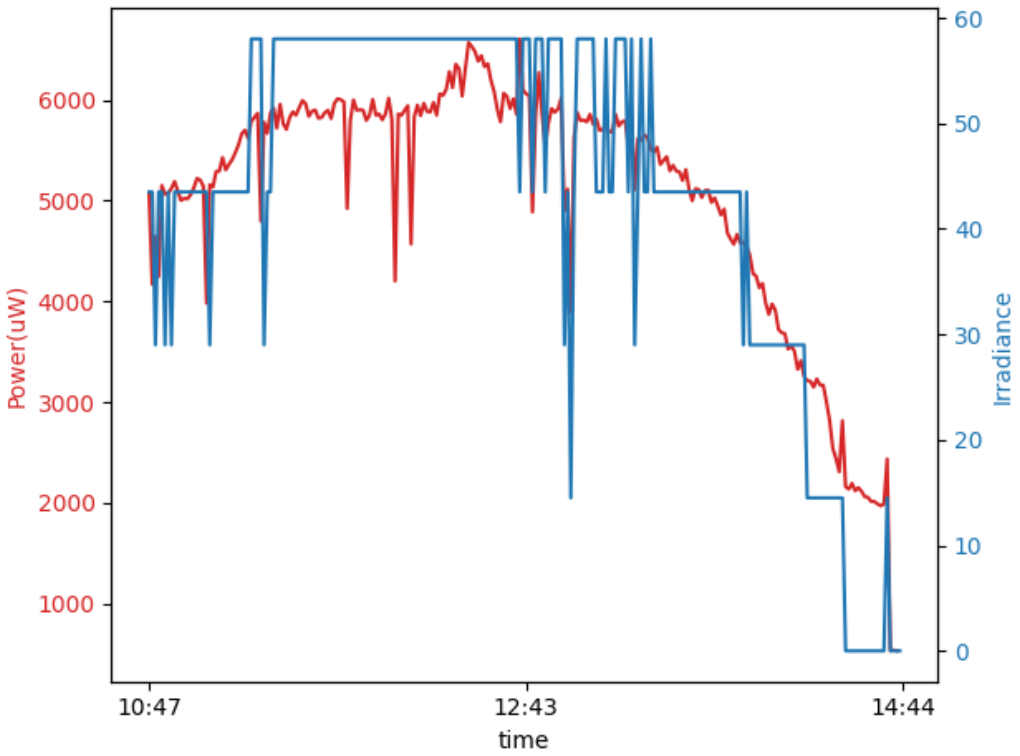

Figure 40: MPP sampling (FOCV) set at 80%. North facing

Direction	MPP (% of V_{oc})	Harvested Energy (mAh)	Mean harvested power (µW)
North	0.80	1.5	5 046
North	0.65	0.85	2 784
South	0.80	11.96	32 463
South	0.65	13.94	35 881

Table 11: Result of outdoor testing.

3.5.4 Conclusion

When comparing the outdoor results, it is noted that the OPV sampled at a FOCV of 65% performs better than those sampling at 80% for higher irradiances. Studying the results of the south side sampling shown in figures 37 and 38, it is shown that the power output for the 80% FOCV sampling and the 65% FOCV sampling has an expected relation as suggested in figure 30, where the power output is about 20% higher for the 65% sampling than for the 80% sampling. One major difference however, is the actual value of the power output for the outdoor results. When, for example, looking at the outdoor results for the 65% sampling, the power output is 60-65 mW for irradiance levels of 800 W/m^2. This compared to the results from the indoor tests in figure 30, which would suggest a power output of 95 mW at an irradiance level of 800 W/m^2. The reason for this could be due to multiple things. Most likely, a reversal of the photoactivation had occurred before the time of the measurements, or that the photoactivation process was incomplete to begin with. Another reason could be an effect of the absorption spectrum of the OPV cell, causing the cell to harvest the energy daylight spectrum differently from the one of the sulfur plasma lamp. Since the sulfur plasma lamp is used in an attempt to simulate daylight it is not regarded to be the root cause for the lower power output in the outdoor testing results. It is also to be noted, that the leads, connecting the OPV to the dev-kit are long, introducing some additional resistance in the system.

When comparing the results from the northern side of the outdoor measurements shown in figures **??** and **??**, it is noticed that the 80% FOCV sampling has a higher power output than the 65% sampling. This is to be expected and in line with the results from the results from the IV curve study explained in section 3.2.3.

It is important to state that a lot of factors can locally have a big effect on the irradiance the OPV cells are experiencing. For example, even if the OPV panels are experiencing the same level of beam radiation, the local reflections from the ground could differ a lot. The individual performance and PCE of each OPV panel could also be different due to heat affected zones on the OPV from bad soldiering.

3.6 Energy Storage Selection

The EHS is not complete until it is decided on how the harvested energy is stored and used. Based on the information provided in section 2.3.5, two different ways of storing power will be presented below and the most appropriate for the application will be chosen.

1. High capacity secondary battery charged by PV

This configuration have some clear advantages, where the already long battery life of a high capacity lithium ion battery will provide the load with power for a long time. Comparing other existing Verisure products, a lithium battery camera and sensor node have a battery life of 3+ years. This means that the a charge cycle will benefit from the total accumulated power outputted from a PV during a whole year. A small capacity lithium battery would on the other hand be much more dependant on the yearly worst case power output experienced during winter with limited light exposure of the PV cell.

2. Super Capacitor charged by PV
Supercapacitors are an interesting technology and have a few clear advantages. One of them being a potential fast charge rate and higher power density. However, since the nodes that are to be powered up by the energy storage unit consume low power and are expected to have relatively long battery lives, these attributes do not have a clear purpose. Combining this with the low power output from the PV cell, the drawbacks of the supercapacitors, such as higher self discharge rates and a non-constant voltage output throughout its charge cycle, needing additional voltage regulation to power the load properly it is assumed that the non-avoidable losses of the system would be to big.

Due to the drawbacks of the supercapacitor discharge and the big advantage of having a battery life greater than one year for the lithium ion battery, the battery is chosen to study further. For most of the battery applications in Verisures' product portfolio, the self discharge rate of supercapacitors would also be a disadvantage.

3.7 OPV Form Factor Selection

Due to design constraints described in section 1.3.1 , the OPV panel will have limitation in terms of its active area. The panels are to reside within a space that limits the area to 55 x 53 mm. However, the construction of the panel is still able to be modified. As the area of the panel is decided, the choice that needs to be made is to determine the number of cells within the panel. These cells are connected in series, meaning that the number of cells will alter the operational voltage of the OPV. Since the energy harvesting IC is decided to be the "Texas Instruments: bq25505" the operational voltage expected in relation to the number of cells can be compared to the efficiency graphs from the "bq25505" data sheet shown in figure 44.

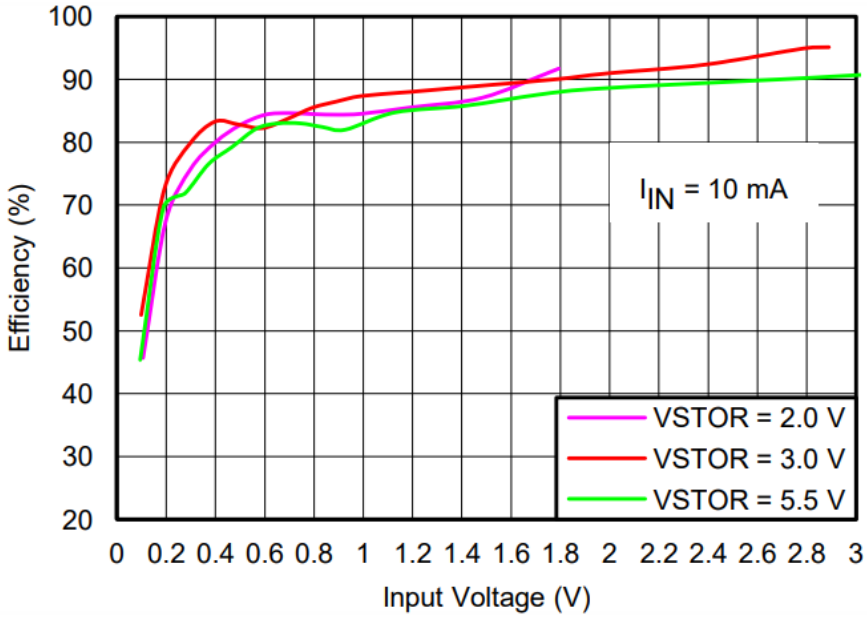

Figure 41: Graph showing the efficiency as a function of the devices' input operational voltage.

By looking at the voltage and current present in STC conditions while working at the MPP shown in figure 20, the voltage provided by each cell can be calculated by dividing the voltage by the number of cells in an OPV panel. The STC curve is generated by a cell with four cells making each cell provide approximately 0.5615 V/Cell knowing that the panel works at 2.246 V at the MPP. A five-cell panel would instead produce 2.8075 V at the MPP. When consulting the bq25505 data sheet it can be seen that the efficiency increase expected when increasing the voltage is 1-2%. The current would also decrease proportionally, theoretically resulting in the same power output. In practice however, the cells in the panels must be separated by 1.5 mm when being produced to ensure that the cells do not short circuit. When going from four to five cells the active area is decreased by 3%. From these calculations it is assumed that the highest overall charging power will be achieved with a 4-cell panel.

In the data sheet, the efficiency is only plotted for specific constant currents, where 10 mA is the closest to the operational current of this panel, meaning that the assumption made above needs to be validated. This can fortunately be done by exploring the efficiency of the "bq25505" when altering between the expected voltage and current inputs for four and five cells, respectively. This test showed that going from four to five cells would yield an actual increase in IC efficiency by 1.2%, but a 3 % decrease in active area, concluding that a four-cell module is a better option.

4 PCB Design

The final EHS consists of multiple components and some of them need to be housed on a PCB. In this section of the rapport this PCB is presented and the key design considerations are explained.

4.1 PCB Design Process Description

The PCB design process is an important part in order to create an efficient EHS. First of all, the relevant IC configuration must be set. This includes the process of identifying the working conditions of the IC and referring to the results in the component evaluation process in section 3 to select a correct configuration of the IC. In this process it is also important to identify the component criteria dictating the quality and choice of electrical components. An overview of this process is described in section 4.2.

The actual design process can then be conducted in a PCB design environment. For this, the program "Altium Designer" was used. This process revolves around consulting the "bq25505" data sheet in order to make well-founded decisions on PCB footprint layout and calculate the correct component values for the intended configuration. The PCB layout is presented in section 4.3 and the schematics are presented in appendix B.

After the PCB has been manufactured, it also needs to be confirmed to work as intended. This is done by connecting the input of the PCB to a power-supply that simulates a PV and a rechargeable battery to the output of the PCB. By measuring the efficiency of the PCB in a range of conditions, its performance can be confirmed. This is presented in section 4.4.1.

4.2 Configuration Component Criteria

The PCB is the intermediate that connects the output from the OPV to the battery input of the rechargeable energy storage. This means that the PCB will house the DC-DC converter and the MPPT regulation. Since this is all featured on the "TI bq25505", designing the OPV is only a matter of implementing the IC to be configured as desired. The IC will be implemented to sample the OPV at 65% of the OCV and with an overcharge protection of 4.2V and a discharge protection of 2.4V.

Regarding components, some must be carefully considered when implemented on the PCB. The capacitance on the VREF_SAMP pin is sensitive for leakage since the voltage over the capacitor dictates at what voltage the MPP will be sampled. The sampling period is 16 seconds meaning that no significant voltage decrease over the capacitance should be present. Therefore a low leakage capacitance is important for a stable MPP performance. [31].

The value of the capacitor between pin VIN_DC and pin VSS is also important to choose correctly. This capacitor initially stores energy from the input source before the energy transfers through the EHS. It is advised to choose a capacitance that is proportional to the capacitance of the input impedance. In figure 9 it becomes clear that the output impedance is mainly resistive. Therefore the minimum recommended value of this capacitor can be used. [31].

Regarding the resistors included in the PCB design, they are only acting as voltage dividers to correctly configure the overcharge/discharge voltage levels and the MPP FOCV sampling voltage. Their value

where therefore calculated and selected according to the instructions in the "TI bq25505" data sheet. A full view of the circuit schematic is shown in appendix B.

4.3 Final PCB Design and Key Design Features

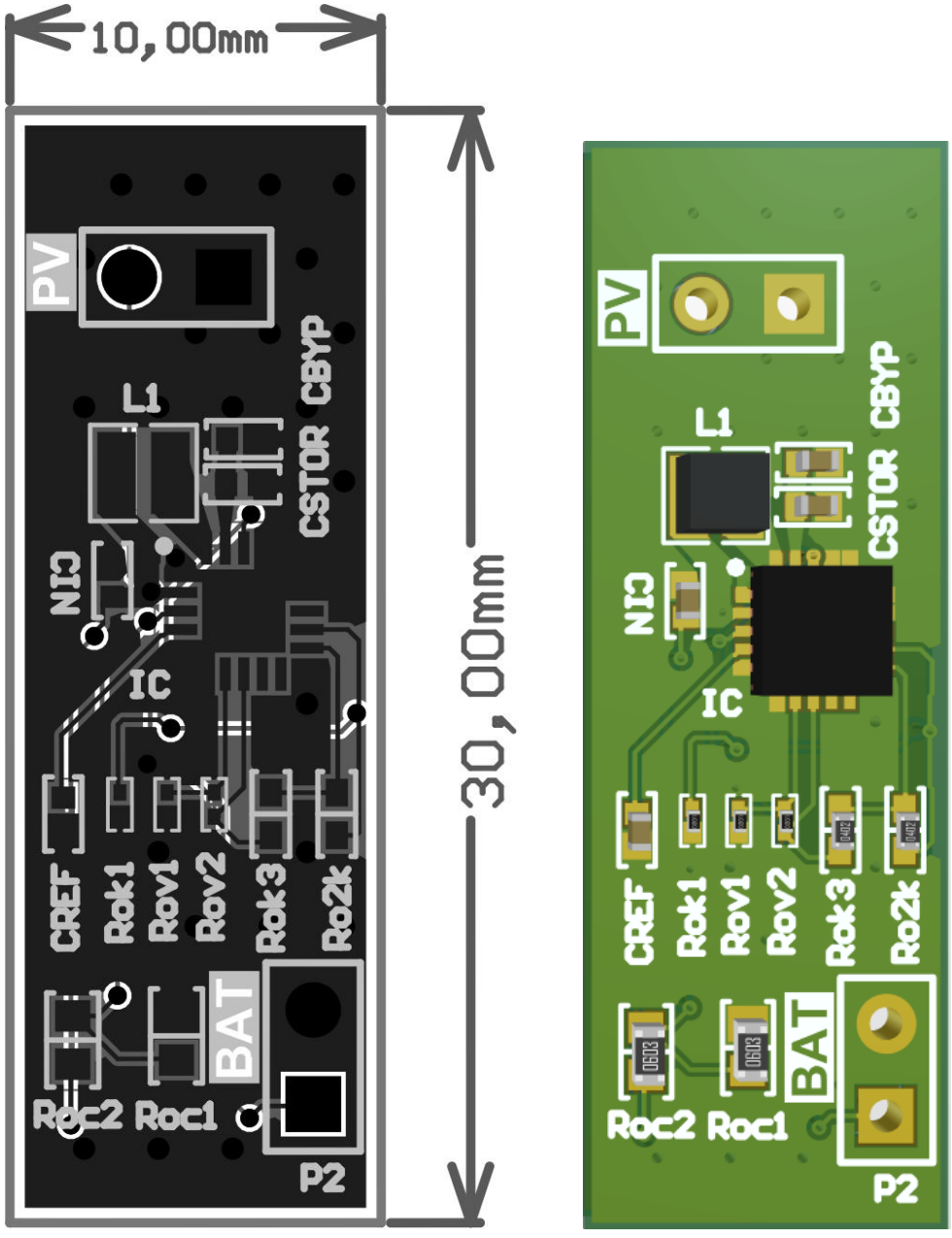

(a) 2d layup **(b)** 3d rendering

Figure 42: Images showing the final PCB design

4.4 PCB Prototype Analysis

4.4.1 PCB Efficiency Testing

To test the performance of the PCB shown in figure 42, the efficiency of the PCB was measured for different power inputs. This was done by measuring the current and voltage at the input of the EHS,

while the bq25505 was sampling the input at a voltage corresponding to 65% of the OCV. At the same time, the charging current and voltage was measured at the terminal of the lithium ion battery being charged. At the time of measuring, the voltage level in the battery was 3.3V. For this experiment, a DC power supply was used to simulate the OPV.

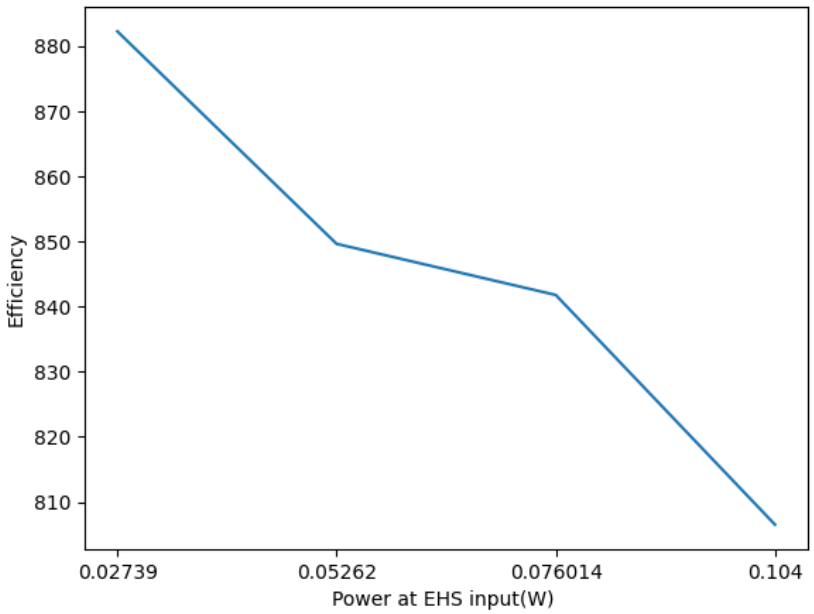

Figure 43: Efficiency of the PCB prototype at different irradiance levels

The input power to the EHS can be directly read from the DC power supply and the charging power can be calculated when knowing the charging current and voltage. This can be measured with a multimeter. The system efficiency will then be the result of dividing the charging power with the OPV output power. In figure 43 the efficiency, calculated at different power output levels, are presented.

The voltage and current outputs from the DC power supply have been chosen with reference to the results of the IV curve study in section 3.2.3. Specifically, simulating an OPV at 200, 400, 600 and 800 W/m^2 after photoactivation are used. The results are presented in figure 43.

It is noticed, when analyzing the results presented in figure 43, that the efficiency tends to decrease for higher irradiance levels. This is not surprising as when the input power to the EHS increases, the efficiency of the EHS decreases [31]. When studying the datasheet of the bq25505 it is also noticed that the efficiency range of the chip for different input voltages, varies a lot. At an input voltage of 2V, the peak efficiency sits at 93%, compared to the peak efficiency of 75% at 0.2V. The open OCV of the OPV however, is 3.1V, so with a FOCV of 65%, the input voltage of the system should be around 2V.

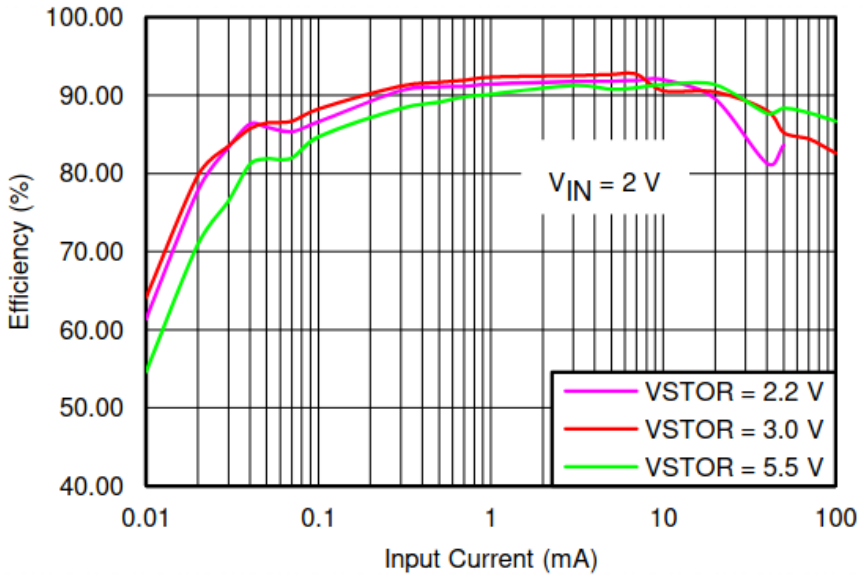

Figure 44: Efficiency of the "bq25505" IC as a function of the input current, at a constant voltage of 2V

In figure 44, the efficiency of the "bq25505" is shown for a constant voltage of 2V. Here it is shown that the even if the "bq25505" is supposed to have a lower efficiency, the efficiency of the EHS is constantly lower for all values of the power input. This might suggest that the EHS has other losses in the circuitry or that losses has been introduced by the measuring setup.

Any leakage of current in the external components will decrease the efficiency of the EHS. When designing the EHS, all of the recommendations for the "bq25505" was followed as closely as possible given the current inventory of the available electrical component vendors. Some compromises had to be done however, and the PCB design had to deviate from the recommended indicators, opting for ones with a more appropriate geometry. This might be a source of leakage. It is also considered that both the leads, connecting the terminal of the rechargeable Li-ion battery and the leads connecting the multimeters might introduce significant resistance to the system, decreasing the efficiency. On average, however, the efficiency is considered high enough, not to redesign anything on the PCB.

5 Power Output and Battery Charging Simulations

As the final EHS is defined, in depth simulations of its performance can be made. These simulations are presented in the section.

5.1 Simulation Process Description

With the EHS defined, its performance can be simulated. This process begins with choosing the solar data correctly and then making the appropriate assumptions necessary to use the information about the EHS.

When all assumptions are set, the actual case studies to simulate must be defined. By referring to older thesis projects conducted at Verisure, information regarding expected battery power drainage could be retrieved and case studies setup. These would be the basis of the simulations.

The simulations can then proceed where Excel and Python were used to get an understanding of the EHS charging performance. The reason for using both Excel and Python for simulations stems from three things. Firstly, the Excel program actually calculates the effective irradiance on a certain plane that can then be used in both the Excel and Python program. This is very useful for locations where the effective irradiance is not available but rather only the local beam, diffuse and reflected irradiation. Secondly, the Excel simulations are not as dynamic as the Python simulations, which can take system aspects, such as PV degradation and an applied draining current, into account. Lastly, since the Python simulations are based on experimental data, the Excel simulation will act as a sanity check to know that the simulations and calculations made with Python are reasonable.

5.2 Simulation Preparations

5.2.1 Selection of Solar Data

In order to calculate good power output and charging estimates of how the EHS will perform in different locations, facing different directions, good solar data must be used. For comparisons sake, it is also important that the data originates from the same database. For this, purpose, data from the "Photovoltaic Geographical Information System" (PVGIS) [20] is used. This database allows different solar data to be extracted. The PVGIS can both extract solar data for a specific location/direction specification in its contributing components on a specified plane as well as the effective irradiance on said plane. With this information, the effective irradiance can be calculated manually in an Excel sheet provided by Henrik Davidsson, senior lecturer at Lund University, or to be used directly as provided by the PVGIS. If simulating locations where the effective data can not be retrieved from PVGIS, the effective irradiation can be calculated via the Excel program as long as the local beam, diffuse and reflective radiation components can be retrieved.

5.2.2 Assumptions Surrounding Simulations

A few assumptions have to be made in order to simulate the charging performance of the EHS. These assumptions will aim to support the different use cases that can be expected when using the EHS.

Firstly, it needs to be noted, that when retrieving the effective irradiance data from PVGIS, it is done by specifying the coordinates and orientation of the plane that the effective irradiance is working on. It is assumed that the effective irradiance is originating from a source normal to this plane. This allows for comparison with the indoor OPV testing done with a light source as explained in section 3.4.2 and is taking advantage of in the Python simulations described in section 5.3.3.

Some assumptions regarding the load powered by the battery also need to be made. First of all, a maximum energy capacity of the rechargeable battery must be set. To make a well-founded decision, data from previous Verisure products have been compared, where it is known that many nodes have been powered by 6 AA sized batteries. Depending on what battery is being used, different energy capacities can be calculated. In this case, a rechargeable AA Li-ion battery is used, corresponding to a total energy storage of around 45 Wh [13].

Regarding the expected energy consumption, it is assumed that the load consumes energy at a constant rate. By determining the time it would take for a battery to fully discharge without any charging, it is possible to determine the total power consumption of the load and self discharge from the battery. Different power consumption rates will be explored since the use case of the EHS is customer specific [14].

The degradation of the OPV cells will have a big impact on the overall charging power provided by the EHS. In section 2.1.5 it is stated that the OPV will experience a burn in period in the initial stages of its lifetime followed by a linear decrease of the PCE. Since it is not known how the panels are handled before being delivered and installed in an EHS, it is assumed that the burn in period is completed upon arrival. Therefore the OPV cells will be simulated using a linear decrease of the PCE. In section 2.1.5 it is also stated that the lifetime of OPV cells that are encapsulated with a flexible barrier film, such as for the provided OPV, are likely to have a lifetime of 10 years or higher. Therefore, it is assumed that the lifetime of the OPV is 10 years, so that the PCE is 80% of its original value at this point.

The use cases that is to be simulated are presented in table12.

Case Study	Battery Size (Wh)	Nominal Battery Life (years)	Power Consumption (mW)
A	45	1	5.13
B	45	2	2.57
C	45	3	1.71
D	45	3	7.38
E	45	3	3.81

Table 12: Different use cases to be simulated

5.2.3 Motivation of Case Studies to Simulate

In table 12 case study A, B, C, D and E is presented. Following is a further explanation of which real world scenarios could create these conditions. The different case studies will be able to correlate to a relevant power consumption that will be an input for the battery charging simulations.

Case study A, B and C represent the use of a detector style node, such as the existing "Cam Pir 3" model from Verisure. It is assumed that the majority of this power consumption is due to excessive use of a high power application or feature on the "Cam Pir 3". All case studies A and B and C are assumed to have lower nominal battery life spans than the 5-year battery life that is Verisures aim for this style of product [14].

Case study D and E correspond to a detector style node with a nominal battery life of 3 years but with the added power consumption of using a hypothetical radar sensor for detection with a high and low sampling frequency, respectively, as suggested by previous thesis works conducted at Verisure [14].

5.3 Simulations

5.3.1 Simulation of OPV Output Using Excel

To simulate the power output from a Solar panel in a specific place parameters defined in 2.2.3 and 2.2.2 are needed.

The solar data components for specific coordinates can be acquired from PVGIS and with the use of inputs such as azimuth, zenith angle and ground reflections all parts of the radiation can be calculated. This is done with the help of equations explained in 2.2.2 and 2.2.3.

After extracting the different components of the radiation equation the use of equation 16 will result in the effective radiation.

To convert this to power output some more information is needed from the system. Specifically the OPV area, OPV efficiency and DC-DC converter efficiency.

$$P = G * OPV_a * OPV_e * DC_e(W) \tag{19}$$

$G =$ Incident light (W/m^2)
$P =$ Power output
$OPV_a =$ OPV active area
$DC_e =$ DC-DC converter efficiency

In some cases the radiation data is presented in the unit Wh/m^2 instead of the preferred W/m^2. If that is the case the amount of sun hours in the radiation data, meaning the amount of hours that the diffuse radiation is not equal to zero, is calculated.

$$P = (G * OPV_a * OPV_e * DC_e)/Sh(W) \tag{20}$$

$Sh =$ Sun hours in a year

Simulating a curved cell can be quite troublesome, therefore the curved cell was simplified into 3 smaller flat cells with different Azimuth angles.

With all this information an simple Excel program can be setup.

Method of the program

- Fill in all the necessary solar data and parameters.
- Arrange all relations and equations in Excel.
- Calculate power output and yearly average irradiance.

Parameters used in simulations Accurate parameters are needed in order to get a good result. These parameters were used for the simulation:

OPV_a= 55 x 53 as described in 3.7
OPV_e= 0.04 As seen from experiments. DC_e= 0.90 described in 3.7
β = 90° representing a device mounted on a vertical wall
γ = -180°,-90°,0°,90° representing north, east, south and west
ρ = 0.20
T = 25° C
Sh = 4559 h
The simulation is done with the latitude and meridian of Lund, Sweden.

Latitude = 55.77°
Meridian = -13.22°
Standard meridian Sweden = -15°

5.3.2 Simulation of OPV Output Using Excel Results

Facing Direction	**Yearly Harvested Energy** (Wh)	**Average Yearly Effective Irradiance** (W/m^2)
S	86	169.7
E	75	146.7
W	67	131.4
N	49	84.8

Table 13: Simulation results using Excel.

Facing Direction	**Flat Cell** (Wh)	**Curved Cell (simulated)** (Wh)
S	86	86
E	75	75
W	67	67
N	44	49

Table 14: Simulation results using Excel with curved and flat cell.

5.3.3 Graphical Simulation of Charging Performance Using Python

In order to simulate how the actual charging performance of a battery will look like, the solar data retrieved from the PVGIS and treated in the Excel program explained in section 5.3.1 can be used. The Excel program is used to calculate the effective irradiance acting on a specific surface and can be used to simulate how a battery can be charged over a period of time. This is done by implementing a Python script that reads the effective irradiance data, calculates the power output from the OPV, accounts for the losses in the EHS and the current drain from the battery, and shows the battery's energy levels over time. An explanation of the Python script follows below and the full script can be found in appendix B.

The effective irradiance hourly solar data for a certain location is retrieved for the north, south, east and west directions and saved in separate Excel sheets. The script reads this data for each direction, respectively, and for each data point the following happens.

- The irradiance data from a direction is read and a corresponding nominal power output is interpolated from values measured during the indoor testing explained in section. 3.4.2.
- The degradation of the OPV due to radiance exposure is accounted for.
- Losses originating from the EHS is subtracted.
- The power output values with all system losses accounted for is saved in an array.
- The power difference between charging power and the power caused by a current draining load is calculated.
- An array tracking the energy level in the battery is updated, adding the power difference to the previous elements energy value.
- Each element in the battery energy level array is compared to the maximum energy rating for the battery and limited if the calculated energy for the element exceeds this value.
- The yearly power harvested, is printed for each direction.
- The lifetime of the battery is printed for each direction.
- The battery energy level array is presented in a plot.

5.3.4 Simulation Results of Charging Performance Using Python

Tables 15 and 16 show the battery lifetime when charged by the EHS based on the Python script that simulates how the EHS charges a battery over time. In figure 45, an example on how the energy level is changed in the battery over time is seen. Examples of the simulated results, for specific case studies and locations are found in appendix C.

Location: Lund, Sweden					
Case Study		**S**	**N**	**E**	**W**
	Load power consumption (mW)	Battery lifetime in years			
A	1.71	10+	10+	10+	10+
B	2.56	10+	10+	10+	10+
C	5.13	10+	2.08	10+	10+
D	7.38	10+	1.04	5.00	6.05
E	3.81	10+	5.93	10+	10+

Table 15: Expected simulated battery life in south, north, east and west directions for irradiance data from Lund, Sweden

Location: Madrid, Spain					
Case Study		**S**	**N**	**E**	**W**
	Load power consumption (mW)	Battery lifetime in years			
A	1.71	10+	10+	10+	10+
B	2.56	10+	10+	10+	10+
C	5.13	10+	3.04	10+	10+
D	7.38	10+	1.17	10+	10+
E	3.81	10+	10+	10+	10+

Table 16: Expected simulated battery life in south, north, east and west directions for irradiance data from Madrid, Spain

Facing direction	**Yearly harvested energy** (Wh)	**Average yearly effective irradiance** (W/m^2)
S	86	169.7
E	66	146.7
W	62	131.4
N	30	84.8

Table 17: Yearly harvested energy based on the Python simulations

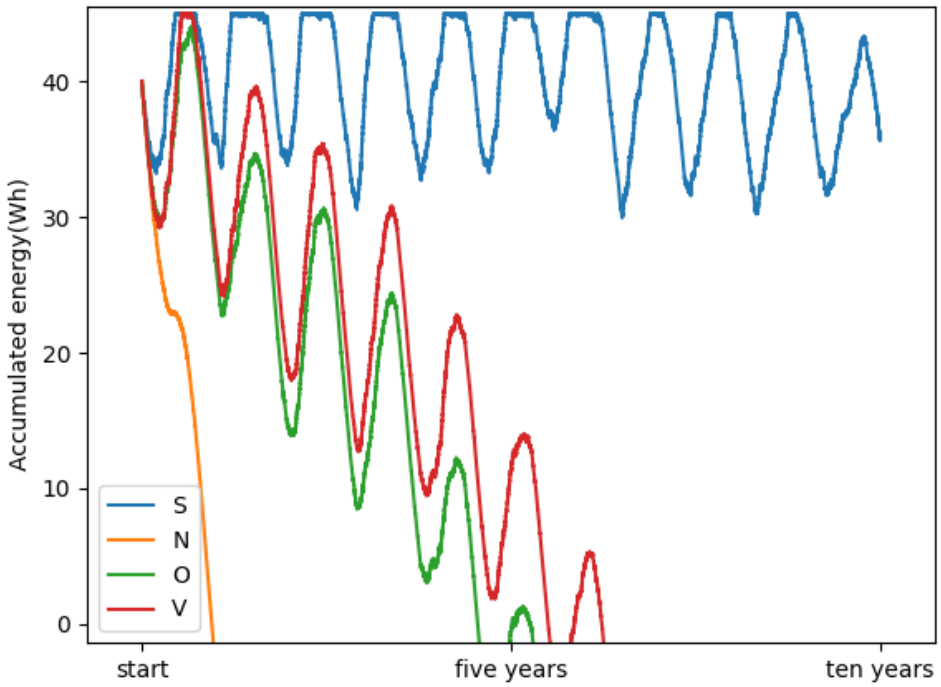

Figure 45: Change of energy level in the battery over time. Location: Lund, Sweden. Case study: D

5.3.5 Discussion on Simulation Results

In section 5.2.2, it is explained that in order to make use of the power output measurements presented in section 3.4.3 in the Python simulation, it must be assumed that the light is incident normal to the simulated surface plane. In the Excel simulation results 5.3.2 two sets of results are presented. One set of results representing a flat OPV panel, and one representing a curved OPV panel. These results are very similar, with only a small difference in the northern direction. This validates the assumption.

In order to simulate the yearly power output of the OPV both the Excel and the Python programs can be used. When comparing the results in table 14 and 17 it is seen that the results are similar. This implies accuracy in both simulation methods. It is noted however, that when comparing the Excel and the Python results for the eastern and western directions, the difference between the simulation results increases compared to the southern direction. The difference increases even more for the northern direction. This might be a result of the Excel program always using the PCE of 4%, which is achieved in STC conditions. The Python simulation instead interpolates between experimental power output values that have been measured and correlated to a certain irradiance level. This would explain why the simulations differ more and more for the directions that are exposed to lower irradiation levels, and therefore experiences conditions less like STC.

The fact that the results from the Excel sheet is the outcome from parameters based on official numbers from the OPV provider and solar data from PVGIS, will act as the sanity check for the Python program. It decreases some of the uncertainty in the simulation that could otherwise be present. The output from the Excel sheet was only compared with the output from the Python program for the location of Lund,

Sweden. After seeing similar results, only the Python program was used to simulate other locations as it is assumed more accurate and visualizes the results for easier interpretation.

When analyzing the results of the Python simulations presented in tables 15 and 16 it is noticed, as assumed, that the geographical location of the EHS and the available irradiance play a big role in the energy harvesting potential. Comparing Lund to Madrid all directions harvested more energy in Madrid. 1.55 times more harvested energy for the south facing EHS, 1.66 times more for the west facing EHS, 1.46 times more for the east facing and 1.2 times more for the north facing EHS. It is interesting to note that the north facing EHS in Lund actually performed proportionally better to the north facing EHS in Madrid, compared to other directions. This is due to Lunds geographically more northern coordinates that lets beam irradiance originate from a source with a slightly northern azimuth angle during summer.

6 Discussion

In this section of the report, an overall discussion will be presented, discussing the overall outcome of the project.

6.1 Conclusions

In regards to the evaluating part of this project including section 3 and 4 in this report the technical evaluation was conducted. It shows that the integration of the EHS is possible without compromising the given design constrictions. This is not surprising as the only real limiting factor was the size of the PCB, that could be implemented to the desired size without problems. It has also been shown that the system efficiency, being the charging power divided by the OPV output power can be kept within a reasonable range working at 88% efficiency at low irradiance levels and 81% for STC conditions. This is in line with the data sheet for the IC where the majority of losses are occurring.

When analysing the design parameters of the EHS and its correlation with the systems performance, it is noted that the ultimate factor deciding the EHS input power is the active area of the OPV. However, if the active area of the OPV is altered, the IC chip evaluation must be redone to ensure that the EHS is working efficiently. Both the voltage and current at the EHS input have a major impact on the efficiency, and an alteration might lead to different IC models to provide the optimal fit for the EHS [31].

Regarding the curvature of the surface of the tested OPV, it is seen that a curved shape can improve power output, but that there is a "sweet spot" meaning there is a optimum radii of the OPV. If no restrictions exist, such as flexibility of the OPV or other inhibiting design factors, the radii should be taken in to consideration as an important part of optimizing the way the OPV is installed.

Overall this project can be seen as successfully completing the task of creating and evaluating the performance of a specific EHS. It was not done without setbacks tough. Equipment malfunction has been the biggest problem during the course of this project, as described throughout the report. This meant that reflecting and analysing results were crucial to draw satisfactory conclusions from them, including checking them for reasonability.

Looking back at one of the initial goal of this project- being able to sustain the battery energy level in a detector device for the duration of the devices' lifetime. The conclusion is that this goal may be reached given the correct circumstances. As presented in tables 15 and 16, many installations seem to be able to sustain the battery life for at least 10 years. The Madrid simulation results in table 16 even suggests that only two out of 20 case studies would fail this criteria.

With the EHS defined as described in this report, the two factors limiting the energy harvesting potential is OPV installation angle, the quality of the installation (sun exposure, shading and such) and the installation specific power consumption of the device. Taking these aspects into account is complex but very important to study further.

6.2 Future Work

The field of solar power is constantly making advances, changing the way its technologies can be used. Different means of extracting the energy potential from light are currently being studied and commercialized. OPV technology has two great advantages. Low production cost and mechanical flexibility- but still it lacks in PCE. Perovskite PV cell is a example of a new emerging PV "thin film" construction that is still flexible but shows promising PCE abilities. While still in its infancy, the highest PCE already exceeds that of the OPV. The Perovskite technology, of course, still have challenges it needs to overcome, such as stability and large scale production capability [6]. For further studies, charting the actual performance and understanding the state of these kinds of technologies should be of great interest in order to keep up to date with the development possibilities of implementing solar technologies. The actual interaction of solar cells and storage elements is also something that can be further studied. The concept of PV integrated batteries is a new concept where the PV cell is directly integrated into the cell structure of a battery [8]. This take on energy harvesting is something that differs a lot from the more common EHS treated in this report. For future studies, it would be interesting to see what such an implementation would result in, in terms of efficiency, robustness and cost.

In term of studies that could be directly succeeding this report, calculations exploring and optimising the battery size can be conducted. Depending on location and the performance of a potential EHS the size of a battery could be decreased, having a positive economical and environmental impact.

References

[1] M. Baradkar. *How do Solar cells work?* Youtube. 2018. URL: https://www.youtube.com/watch?v=L_q6LRgKpTw.

[2] BatteryGuy. *Supercapacitors versus batteries*. 2020. URL: https://batteryguy.com/kb/knowledge-base/supercapacitors-versus-batteries/.

[3] C. Deziel. *The Effect of Wavelength on Photovoltaic Cells*. https://sciencing.com/effect-wavelength-photovoltaic-cells-6957.html, 2020.

[4] A. Dolara, G. di Fazio, S. Leva, G. Manzolini, R. Simonetti, and A. Terenzi. *Outdoor Assessment and Performance Evaluation of OPV Modules*. Vol. 11. 2. 2021, pp. 391–399. DOI: 10.1109/JPHOTOV.2021.3052767.

[5] J. Duffie and W. Beckman. *Solar engineering of thermal processes*. Second copy. John Whiley Sons, Inc., 1991.

[6] O. of Energy Efficiency Renewable Energy. *Perovskite Solar Cells- Solar Energy Technologies Office*. URL: https://www.energy.gov/eere/solar/perovskite-solar-cells.

[7] N. Forsgren. *Wieland System Design Description*. English. Version 2. Epishine. 17 pp. November 2, 2021.

[8] A. Gurung and Q. Qiao. *Solar Charging Batteries: Advances,Challenges, and Opportunities*. Vol. 2. 2018, pp. 1217–1230.

[9] *Highly efficient, regulated dual-output, ambient energy manager for up to 7-cell solar panels with optional primary battery*. AEM10941. E-peas Semiconductors. 2021.

[10] *Highly Versatile Buck-Boost Ambient Energy Manager Battery Charger For Up to 7-cell Solar Panels*. AEM10300. E-peas Semiconductors. 2021.

[11] R. Keim. *The PN Junction Diode and Diode Characteristics*. 2020. URL: https://www.allaboutcircuits.com/video-tutorials/the-pn-junction-and-the-diode/.

[12] B. Kippelen and J.-L. Brédas. *Organic photovoltaics*. https://pubs.rsc.org/en/content/articlehtml/2009/ee/b812502r 2008.

[13] *Kjell Company 18650 Li-ion-batteri 3,6 V 2600 mAh*. https://www.kjell.com/se/produkter/kontor/batterier/laddningsbara-batterier/litium-ion-batterier/kjell-company-18650-li-ion-batteri-36-v-2600-mah-p32058. Accessed: 2021-12-08.

[14] I. Larsson and G. Plomgren. "Microwave Radar Implementation in Outdoor Home Alarm Systems". Accessed: 2021-12-08. MA thesis.

[15] J. Libich, J. Máca, J. Vondrák, O. Čech, and M. Sedlaříková. *Supercapacitors: Properties and applications*. Vol. 17. 2018, pp. 224–227. DOI: https://doi.org/10.1016/j.est.2018.03.012.

[16] B. Ling, Q. S. Han, J. Li, F. Li, Q. Wang, and Xiaohong. "On-Site Traversal Fractional Open Circuit Voltage with Uninterrupted Output Power for Maximal Power Point Tracking of Photovoltaic Systems". In: *Electronics* 9.11 (2020). ISSN: 2079-9292. DOI: 10.3390/electronics9111802.

[17] A. Manthiram. *An Outlook on Lithium Ion Battery Technology*. 2017. URL: https://pubs.acs.org/doi/full/10.1021/acscentsci.7b00288.

[18] M. M. B. McGehee. *Progress in Understanding Degradation Mechanisms and Improving Stability in Organic Photovoltaics*. 2017. DOI: DOI:10.1002/adma.201603940.

[19] T. Olofsson. *Energy Harvesting with Solar Cells for Wireless Alarm Nodes*. URL: https://lup.lub.lu.se/student-papers/search/publication/8959130.

[20] *Photovoltaic Geographical Information System-interactive tools*. https://re.jrc.ec.europa.eu/pvg_tools/en/#MR. Accessed: 2021-12-06.

[21] R. Rawat and S. S. Chandel. *Hill climbing techniques for tracking maximum power point in solar photovoltaic systems - A review*. 2013.

[22] A. Sellinger. *Advanced Electron Transport Materials for Application in Organic Photovoltaics (OPV)*. Youtube. 2014. URL: https://www.youtube.com/watch?v=EVGV9TOt8y8.

[23] H. Sharma, A. Haque, and Z. A. Jaffery. "An Efficient Solar Energy Harvesting System for Wireless Sensor Nodes". In: *2018 2nd IEEE International Conference on Power Electronics, Intelligent Control and Energy Systems (ICPEICES)*. 2018, pp. 461–464. DOI: 10.1109/ICPEICES.2018.8897434.

[24] A. Smets. *7.3 - MPPT*. 2013. URL: https://www.youtube.com/watch?v=0ItjKs7aJFM&t=884s (visited on 11/04/2021).

[25] A. Smets. *WLearn Solar Energy | Series and Shunt Resistance*. 2019. URL: https://www.youtube.com/watch?v=MIxPkWBHsCw.

[26] R. Søndergaard, M. Hösel, D. Angmo, T. T. Larsen-Olsen, and F. C. Krebs. *Roll-to-roll fabrication of polymer solar cells*. Vol. 15. 1. 2012, pp. 36–49. DOI: https://doi.org/10.1016/S1369-7021(12)70019-6. URL: https://www.sciencedirect.com/science/book/pii/S1369702112700196.

[27] E. Spooner. "A PhD Student Condenses: Factors Influencing OPV Stability". PhD thesis. University of Sheffield, 2018.

[28] Swagatam. *How Boost Converters Work*. URL: https://www.homemade-circuits.com/how-boost-converters-works/.

[29] S. Thil. *Representation of azimuth and zenith angles*. www.researchgate.net. URL: https://www.researchgate.net/figure/Representation-of-azimuth-and-zenith-angles_fig1_299413323.

[30] T. O. C. Tutor. *Boost Converters - DC to DC Step Up Voltage Circuits*. 2019. URL: https://www.youtube.com/c/TheOrganicChemistryTutor/featured.

[31] *ultra low-power boost charger with battery management and autonomous power multiplexer for primary battery in energy harvester applications*. bq25505. Texas Instruments. Mar. 2019.

[32] WaveformLightning. *What is the difference between lux and lumens?* URL: https://www.waveformlighting.com/home-residential/what-is-the-difference-between-lux-and-lumens.

[33] N. D. Weimar. *Standard Test Conditions (STC)-definition and problems*. https://sinovoltaics.com/. 2017. URL: https://sinovoltaics.com/learning-center/quality/standard-test-conditions-stc-definition-and-problems/.

[34] B. Zaidi. *Solar Panels and Photovoltaic Materials*. IntechOpen, 2018, pp. 2–5.

Appendix A

Listing 1: Power_Output_Calculator.py

```
import matplotlib.pyplot as plt
import numpy as np
import pandas as pd
from sys import argv

# The irradiance data from a direction is read and relevant global arrays
# are initialized
df_S = pd.read_excel(r'/home/kristoffer/Dokument/effective_irradiance_data_S_' \
+ argv[3] + '.xlsx', sheet_name='Sheet1')
effective_irr_S = df_S.to_numpy()
df_N = pd.read_excel(r'/home/kristoffer/Dokument/effective_irradiance_data_N_' \
+ argv[3] + '.xlsx', sheet_name='Sheet1')
effective_irr_N = df_N.to_numpy()
df_V = pd.read_excel(r'/home/kristoffer/Dokument/effective_irradiance_data_V_' \
+ argv[3] + '.xlsx', sheet_name='Sheet1')
effective_irr_V = df_V.to_numpy()
df_O = pd.read_excel(r'/home/kristoffer/Dokument/effective_irradiance_data_O_' \
+ argv[3] + '.xlsx', sheet_name='Sheet1')
effective_irr_O = df_O.to_numpy()
power_output_array_S = np.zeros(np.size(effective_irr_S))
battery_energy_level_array_S = np.zeros(np.size(effective_irr_S))
power_output_array_N = np.zeros(np.size(effective_irr_N))
battery_energy_level_array_N = np.zeros(np.size(effective_irr_N))
power_output_array_V = np.zeros(np.size(effective_irr_V))
battery_energy_level_array_V = np.zeros(np.size(effective_irr_V))
power_output_array_O = np.zeros(np.size(effective_irr_O))
battery_energy_level_array_O = np.zeros(np.size(effective_irr_O))


# This function is declared to output the harvested energy during the inputted
# number of years
def acumulate_power(years):
    datapoints = 8760 * years
    i = 0
    while i < datapoints:
        acc_pow_array = [power_output_array_S[0: i].sum(), \
        power_output_array_N[0: i].sum(),
                         power_output_array_V[0: i].sum(), \
                         power_output_array_O[0: i].sum()]
        i = i + 1
    return acc_pow_array


# This function is declared to take the inputted base current and subtracts
# it to the power output array in order to track how the energy level in
# a potential battery changes
# over time
def generate_battery_energy_levels(base_current):
    i = 0
    LifeTime_S = 0
    LifeTime_N = 0
    LifeTime_O = 0
    LifeTime_V = 0
    battery_energy_level_array_S[0] = 40
    battery_energy_level_array_N[0] = 40
    battery_energy_level_array_O[0] = 40
    battery_energy_level_array_V[0] = 40
    first = 1
```

```
    while i < battery_energy_level_array_S.size:
        if i > 0:
            diff = power_output_array_S[i] - base_current
            energy_at_i = battery_energy_level_array_S[i - 1] + diff
            if diff ≤ 0:
                battery_energy_level_array_S[i] = energy_at_i
            if diff > 0 and int(battery_energy_level_array_S[i - 1]) < 45:
                battery_energy_level_array_S[i] = energy_at_i
            if energy_at_i ≥ 45:
                battery_energy_level_array_S[i] = 45
                if energy_at_i ≤ 0 and first == 1:
                    first = 0
                    LifeTime_S = i / 8760
        i = i + 1
    i = 0
    first = 1
    while i < battery_energy_level_array_N.size:
        if i > 0:
            diff = power_output_array_N[i] - base_current
            energy_at_i = battery_energy_level_array_N[i - 1] + diff
            if diff ≤ 0:
                battery_energy_level_array_N[i] = energy_at_i
            if diff > 0 and int(battery_energy_level_array_N[i - 1]) < 45:
                battery_energy_level_array_N[i] = energy_at_i
            if energy_at_i ≥ 45:
                battery_energy_level_array_N[i] = 45
            if energy_at_i ≤ 0 and first == 1:
                first = 0
                LifeTime_N = i / 8760

        i = i + 1
    i = 0
    first = 1
    while i < battery_energy_level_array_O.size:
        if i > 0:
            diff = power_output_array_O[i] - base_current
            energy_at_i = battery_energy_level_array_O[i - 1] + diff
            if diff ≤ 0:
                battery_energy_level_array_O[i] = energy_at_i
            if diff > 0 and int(battery_energy_level_array_O[i - 1]) < 45:
                battery_energy_level_array_O[i] = energy_at_i
            if energy_at_i ≥ 45:
                battery_energy_level_array_O[i] = 45
            if energy_at_i ≤ 0 and first == 1:
                first = 0
                LifeTime_O = i / 8760
        i = i + 1
    i = 0
    first = 1
    while i < battery_energy_level_array_V.size:
        if i > 0:
            diff = power_output_array_V[i] - base_current
            energy_at_i = battery_energy_level_array_V[i - 1] + diff
            if diff ≤ 0:
                battery_energy_level_array_V[i] = energy_at_i
            if diff > 0 and int(battery_energy_level_array_V[i - 1]) < 45:
                battery_energy_level_array_V[i] = energy_at_i
            if energy_at_i ≥ 45:
                battery_energy_level_array_V[i] = 45
            if energy_at_i ≤ 0 and first == 1:
                first = 0
                LifeTime_V = i / 8760
        i = i + 1
```

```
122
123     return LifeTime_S, LifeTime_N, LifeTime_O, LifeTime_V
124
125 # This function is declared to use the measured power output values, measured
126 # at different irradiances and
127 # interpolates the inputted irradiance level values to output a corresponding
128 #power output. The system losses is also accounted for at this stage.
129 def interpolate(irr):
130     power_output = 0
131     if irr < 200:
132         power_output = irr / 200 * 26073 / 1000000 * int(argv[1]) / 100
133
134     if 200 ≤ irr < 400:
135         power_output = irr / 400 * 46714 / 1000000 * int(argv[1]) / 100
136
137     if 400 ≤ irr < 600:
138         power_output = irr / 600 * 66775 / 1000000 * int(argv[1]) / 100
139
140     if 600 ≤ irr < 800:
141         power_output = irr / 800 * 85138 / 1000000 * int(argv[1]) / 100
142
143     if 800 ≤ irr < 1000:
144         power_output = irr / 1000 * 92000 / 1000000 * int(argv[1]) / 100
145
146     if irr ≥ 1000:
147         power_output = 92000 / 1000000 * int(argv[1]) / 100
148
149     return power_output
150
151 # This function takes the inputted results and visualises it in a graph.
152 # It also prints the yearly power that has been harvested and the
153 # expected time before the battery runs out of stored energy
154 def visualize_results(results):
155     Results = results
156     print("S   N    O   V")
157     print("yearly power generation(Wh)")
158     print(acumulate_power(1))
159     print("expected lifetime(years)")
160     print(Results)
161     fig = plt.figure()
162     ax = fig.add_axes([0.15, 0.1, 0.8, 0.8])  # main axes
163     ax.set_xticks(
164         [0, np.array(battery_energy_level_array_S).size / 2, \
165         np.array(battery_energy_level_array_S).size])
166     ax.set_xticklabels(['start', 'five years', 'ten years'])
167     plt.plot(battery_energy_level_array_S, label="S")
168     plt.plot(battery_energy_level_array_N, label="N")
169     plt.plot(battery_energy_level_array_O, label="O")
170     plt.plot(battery_energy_level_array_V, label="V")
171     plt.ylabel("Accumulated energy(Wh)")
172     plt.legend()
173     plt.show()
174
175
176 # This function uses the "interpolate()" function in order to generate
177 # an array where the hourly power generation is
178 # stored. At this stage, the degradation of the OPV is taken into account.
179 def generate_power_output_arrays(degradation_factor):
180     i = 0
181     for irr in effective_irr_S:
182         power_output_array_S[i] = interpolate(irr) * (1 - degradation_factor * i)
183         i = i + 1
184
```

```
    i = 0
    for irr in effective_irr_N:
        power_output_array_N[i] = interpolate(irr) * (1 - degradation_factor * i)
        i = i + 1
    i = 0
    for irr in effective_irr_V:
        power_output_array_V[i] = interpolate(irr) * (1 - degradation_factor * i)
        i = i + 1

    i = 0
    for irr in effective_irr_O:
        power_output_array_O[i] = interpolate(irr) * (1 - degradation_factor * i)
        i = i + 1


# The main function calls the relevant functions.
def main():
    degradation_factor = 2.2831 / 1000000
    generate_power_output_arrays(degradation_factor)
    results = generate_battery_energy_levels(float(argv[2]))
    visualize_results(results)


if __name__ == "__main__":
    if len(argv) == 4:
        main()
    else:
        print("Input syntax should be python3 Power_Output_Calculator.py \
        [system efficiency in percent] "
              "[battery current consumption in W] [location in lower case]")
        print("Example input: python3 Power_Output_Calculator.py 81 \
        0.001887731481481 malm ")
```

Appendix B

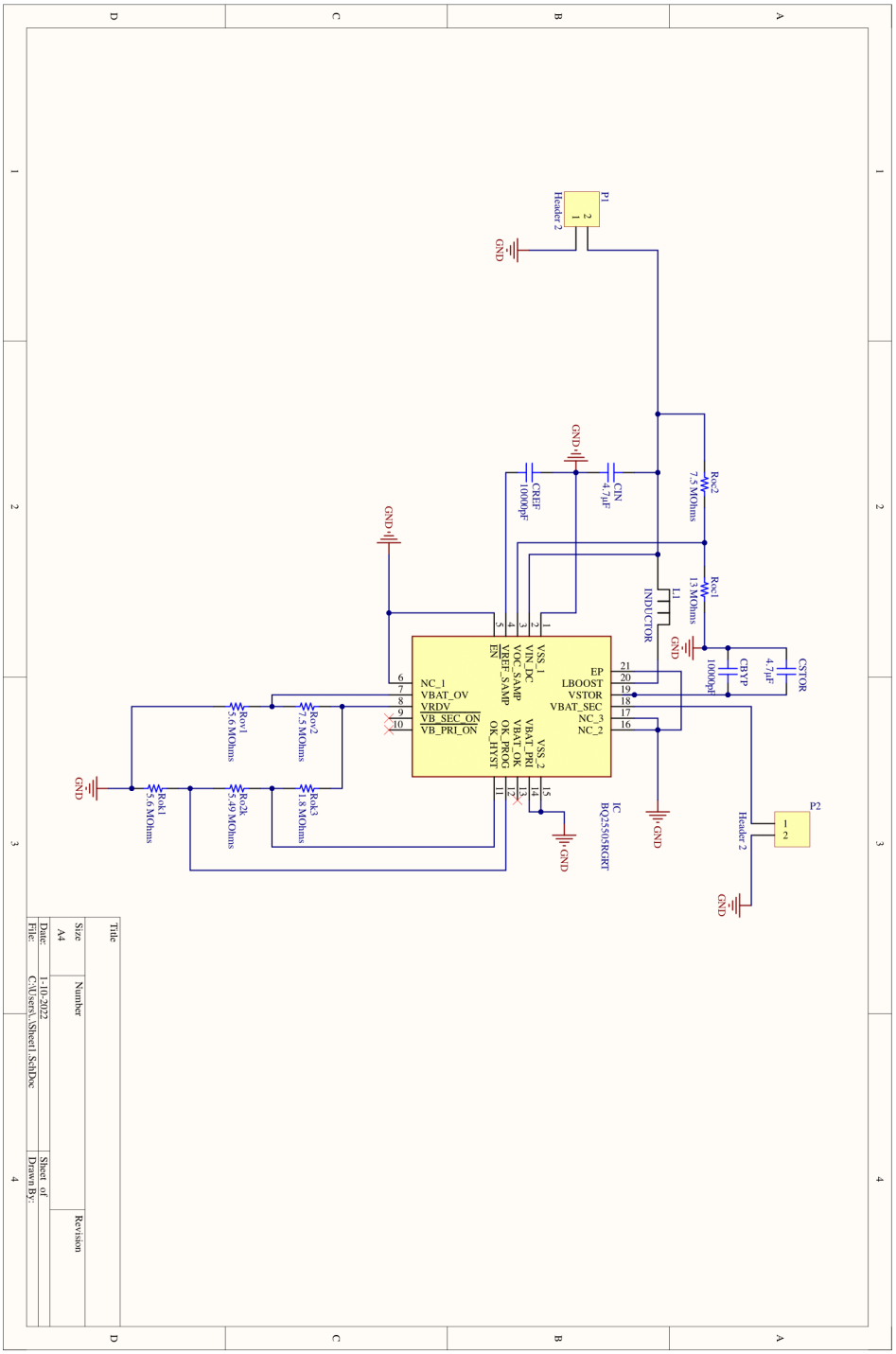

Figure 46: Final PCB schematic.

Appendix C

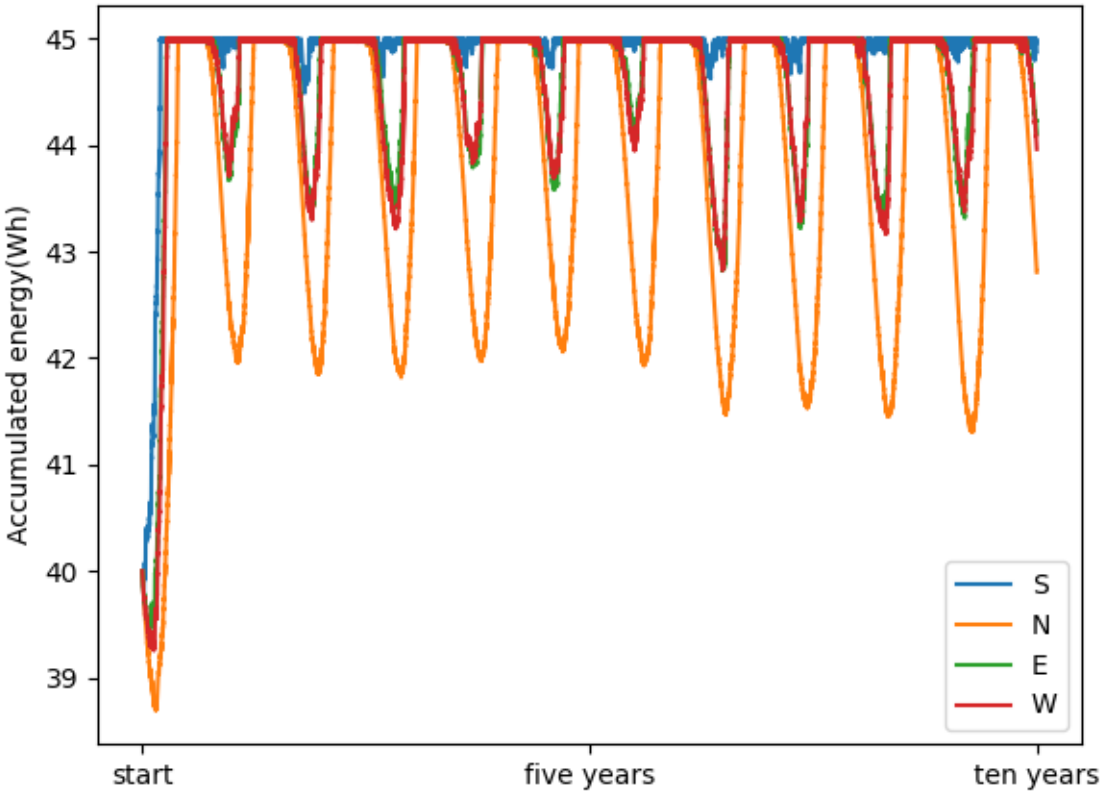

Figure 47: Graphical output from Python simulation. Case study: A. Location: Lund.

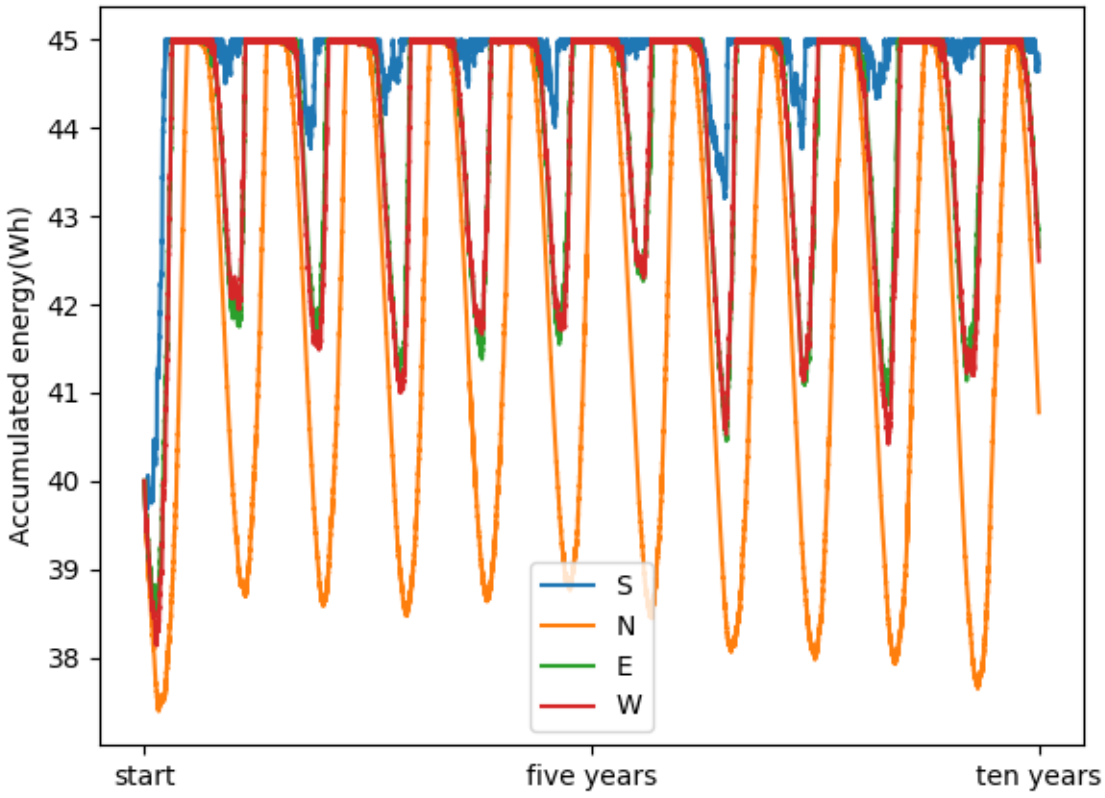

Figure 48: Graphical output from Python simulation. Case study: B. Location: Lund.

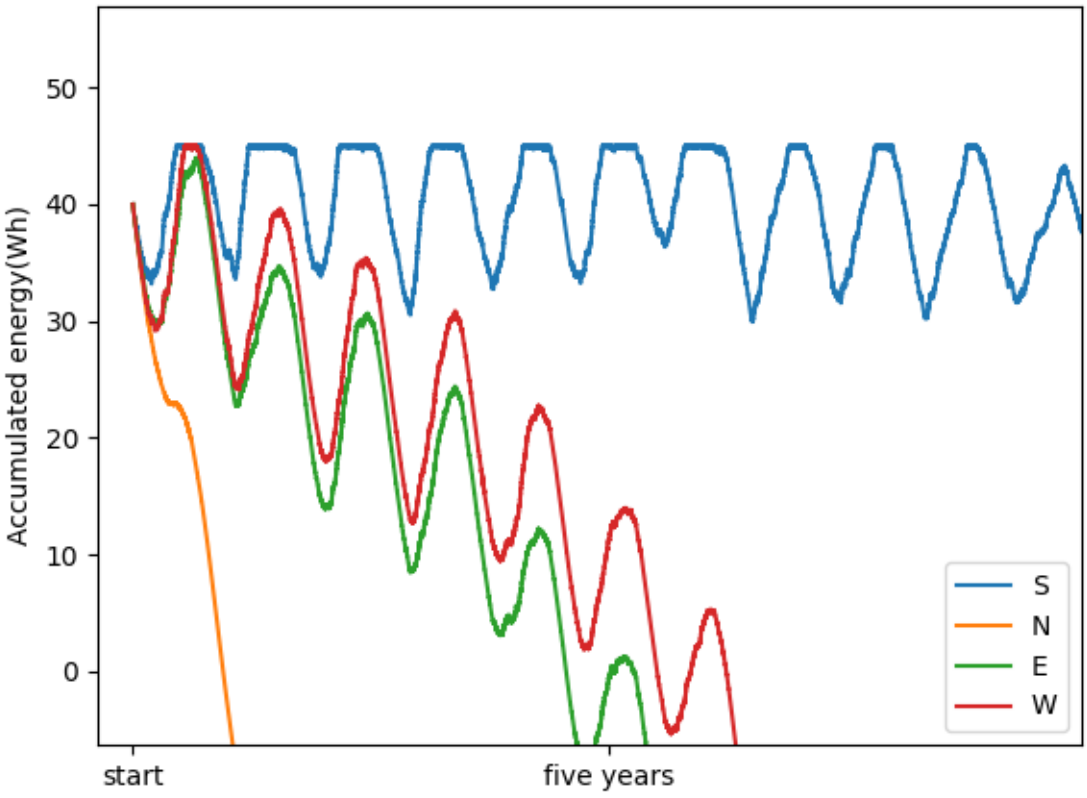

Figure 49: Graphical output from Python simulation. Case study: D. Location: Lund.

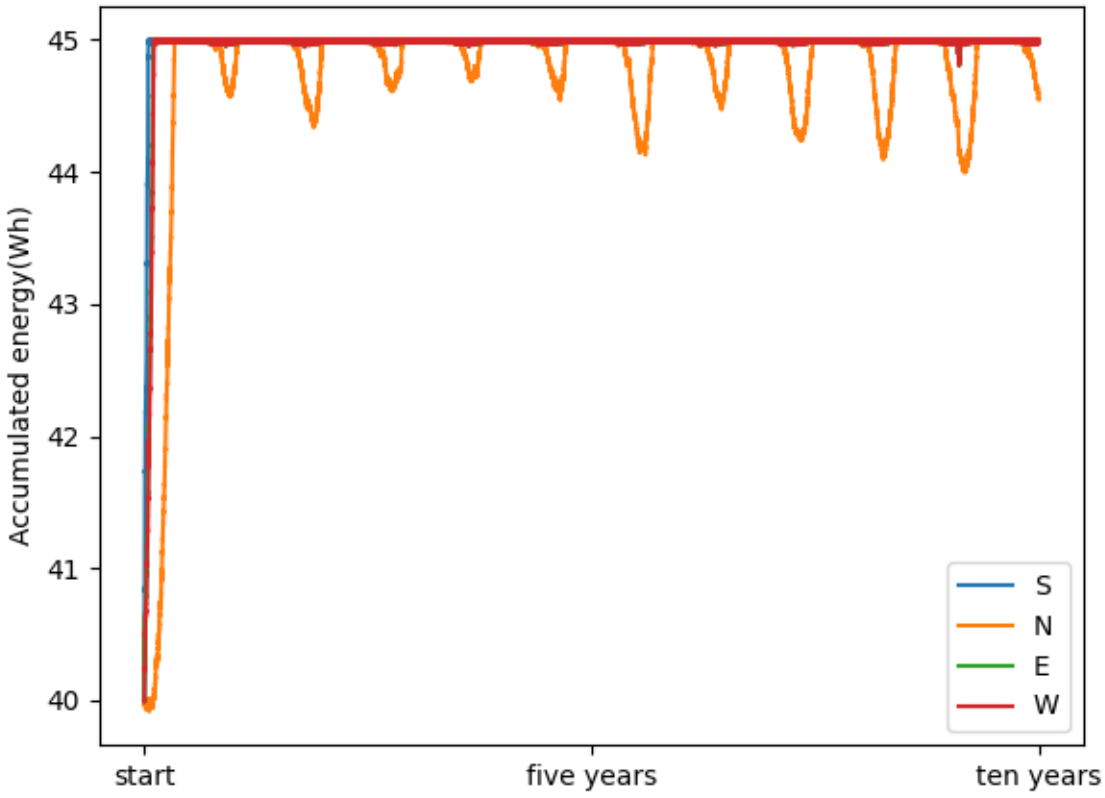

Figure 50: Graphical output from Python simulation. Case study: A. Location: Lund.

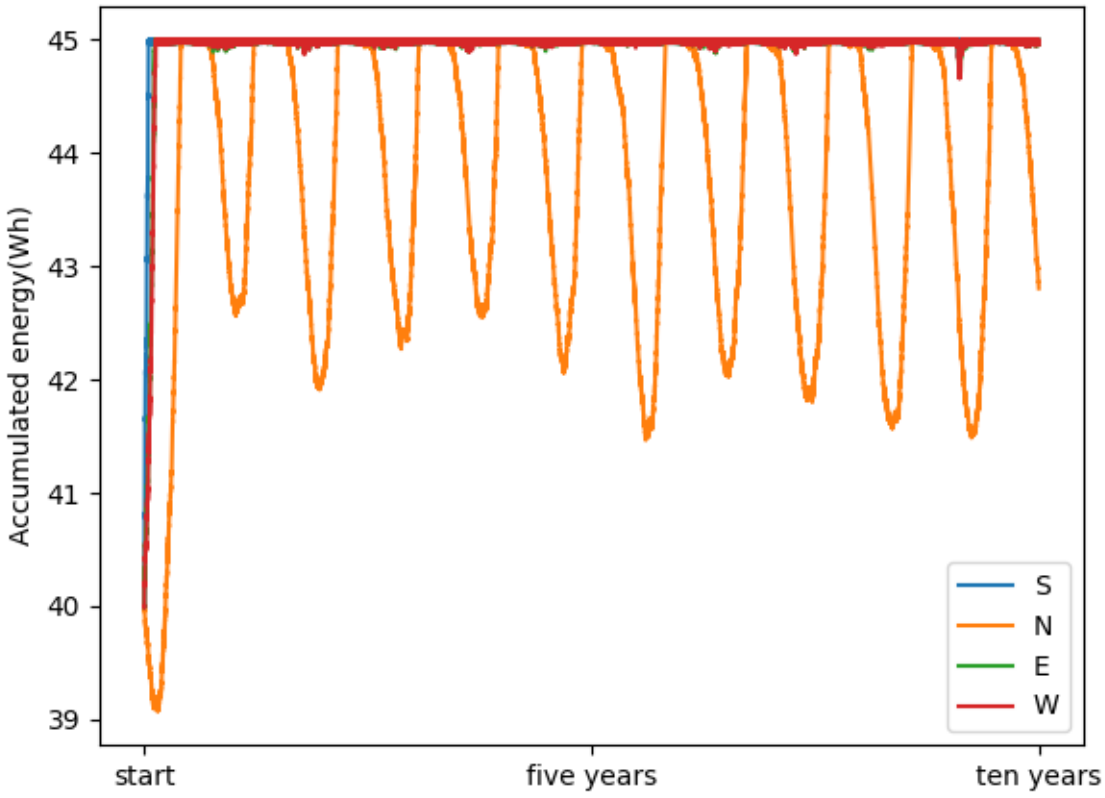

Figure 51: Graphical output from Python simulation. Case study: B. Location: Lund.

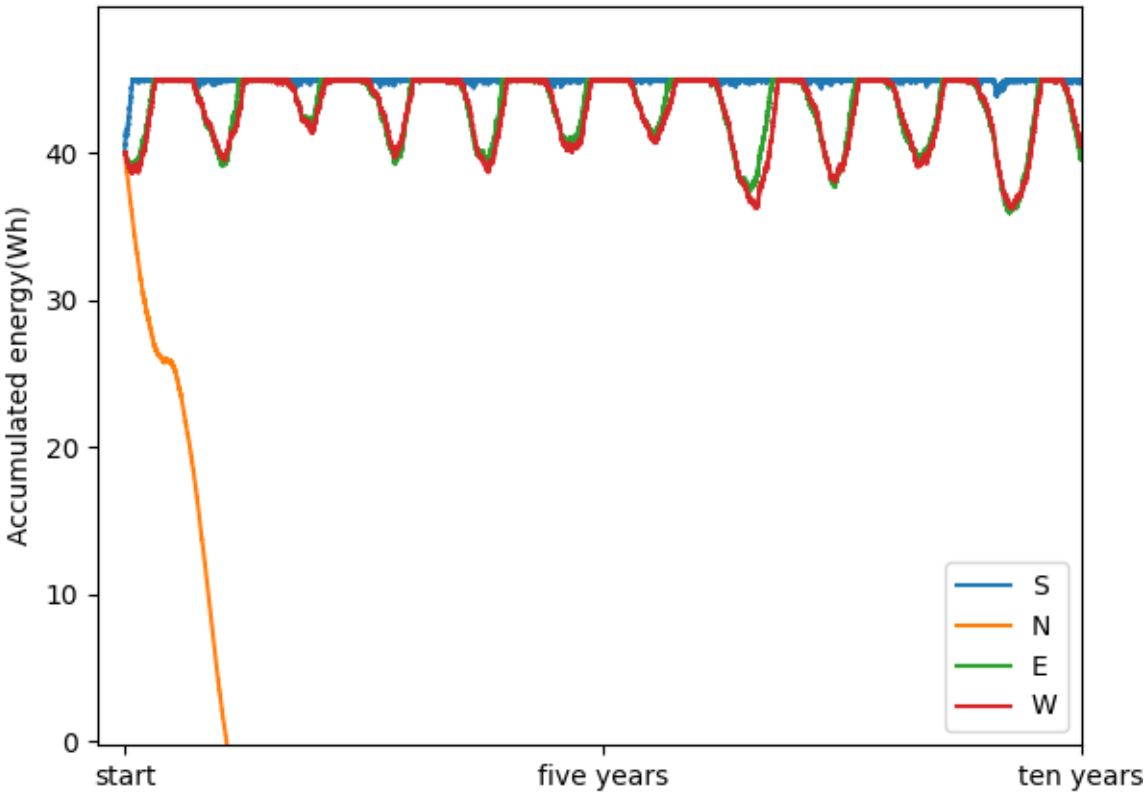

Figure 52: Graphical output from Python simulation. Case study: D. Location: Lund.